Molecular dynamics simulation study of the ejection and transport of polymer molecules in matrix-assisted pulsed laser evaporation

Elodie Leveugle and Leonid V. Zhigilei[a)]
Department of Materials Science and Engineering, University of Virginia, 395 McCormick Road, Charlottesville, Virginia 22904-4745, USA

(Received 23 April 2007; accepted 31 July 2007; published online 11 October 2007)

The physical mechanisms and molecular-level picture of laser-induced material ejection from frozen solutions of polymer molecules in a volatile matrix are investigated in a series of coarse-grained molecular dynamics simulations. The simulations are performed for polymer concentrations up to 6 wt % and laser fluences covering the range from the regime where molecular ejection is limited to matrix evaporation from the surface up to more than twice the threshold fluence for the onset of the collective molecular ejection or ablation. The results of the simulations are related to experimental observations obtained in matrix-assisted pulsed laser evaporation (MAPLE) thin film depositions and are used to address unresolved research questions that are of direct relevance to MAPLE performance. Contrary to the original picture of the ejection and transport of individual polymer molecules in MAPLE, the simulations indicate that polymer molecules are only ejected in the ablation regime and are always incorporated into polymer-matrix clusters/droplets generated in the process of the explosive disintegration of the overheated matrix. The entanglement of the polymer molecules facilitates the formation of intricate elongated viscous droplets that can be related to the complex morphologies observed in polymer films deposited by MAPLE. Analysis of the state of the irradiated target reveals a substantial increase of the polymer concentration and complex surface morphology generated in the new surface region by the ablation process. The ramifications of the computational predictions for interpretation of experimental data and the directions for future experimental exploration are discussed based on the physical picture of molecular ejection and transport in MAPLE emerging from the simulations. © *2007 American Institute of Physics*. [DOI: 10.1063/1.2783898]

I. INTRODUCTION

Matrix-assisted pulsed laser evaporation (MAPLE) is a technique developed with a goal of achieving a soft molecule-by-molecule deposition of high-quality ultrathin organic, bioorganic, and composite films with minimum chemical modification of the target material.[1–6] In this technique, the laser target is prepared by dissolving the material to be deposited in a volatile solvent (matrix) that readily absorbs laser light. A homogeneous dilute solution (typically up to several wt %) is then frozen and placed into a vacuum chamber for deposition. In MAPLE deposition of polymer films, short pulse laser irradiation of the target results in a collective ejection or ablation of the matrix which entrains the polymer molecules along into the plume. The ejected polymer molecules are deposited on a substrate, whereas the volatile solvent molecules are pumped away from the deposition chamber. Since most of the laser energy is absorbed by the volatile matrix rather than polymer molecules, the photochemical decomposition of polymers can be minimized or even completely eliminated. Moreover, since the ablation onset in MAPLE is defined by the thermodynamic parameters of the volatile solvent rather than the polymeric material, deposition can proceed at significantly lower, as compared to the conventional pulsed laser deposition (PLD) technique, energy densities, minimizing thermal decomposition of the polymer molecules.

First investigations have demonstrated that with an appropriate choice of experimental parameters (laser wavelength, fluence and pulse duration, type of solvent, target and substrate temperature, and background gas pressure) MAPLE is capable of providing conditions for "soft" ejection and deposition of polymer and biological molecules without significant modification of the chemical structure and functionality. A broad range of MAPLE applications include deposition of polymer thin films for optoelectronic and chemical sensor applications,[7–11] growth of active protein thin films,[12–16] polymer-carbon nanotube composites,[4,17,18] and films consisting of nanoparticles.[19] Evaluation of the performance of resonant infrared MAPLE (Refs. 20–22) and exploration of water ice as a MAPLE matrix[14,16,23–26] are some of the new directions that have potential for further expanding the range of applicability of this technique.

While the area of MAPLE applications is rapidly expanding, the understanding of the fundamental processes responsible for the molecular transfer remains poor. The initial picture of the ejection and transport of individual polymer molecules in MAPLE (Refs. 1–3) comes into conflict with the results of high-resolution scanning electron microscopy (SEM) and atomic force microscopy (AFM) imaging of MAPLE deposited films. The AFM and SEM images reveal

[a)]Author to whom correspondence should be addressed. Electronic mail: lz2n@virginia.edu

 © 2007 American Institute of Physics

Downloaded 11 Oct 2007 to 128.143.68.241. Redistribution subject to AIP license or copyright, see http://jap.aip.org/jap/copyright.jsp

significant surface roughness, with well-defined aggregates or clusters with characteristic sizes ranging from tens of nanometers to tens of microns.[11,14,18,24,25,27–30] The morphology of the deposited films exhibits strong dependence on the temperature of the substrate[25,27] and sometimes contains distinct wrinkled surface features[18,30] consistent with a scenario in which a significant amount of volatile solvent reaches the substrate and evaporates leaving behind characteristic polymer structures.[18,30–32] The formation of large polymer features on the substrate is rather unexpected since the original polymer concentration in the target is low and polymer molecules are dissolved in the matrix down to the molecular level. Moreover, the entrainment of the polymer molecules in the expanding plume of the volatile matrix does not provide an environment suitable for condensation of polymer clusters.

The results on the rough surface morphology of the deposited films, therefore, call for revisiting the physical picture of the molecular transfer in MAPLE. A better understanding of the relation between the basic mechanisms of laser interaction with the target material, nonequilibrium processes caused by the fast deposition of laser energy, parameters of the ejected ablation plume, and the resulting morphological characteristics of the growing film would be very helpful for optimization of the experimental parameters in current applications of MAPLE as well as the emergence of new areas of application of this technique. To date, however, there have been virtually no theoretical or computational efforts aimed specifically at obtaining a better understanding of MAPLE and the exploration of the multidimensional space of experimental parameters has been done largely empirically.

Molecular-level computer modeling has a good potential of revealing the mechanisms of molecular ejection and transport in MAPLE. In particular, atomic-level molecular dynamics (MD) simulations have been successfully applied to investigation of the rates and channels of the energy transfer from matrix to an embedded polymer molecule,[33–35] as well as the conformational changes in the polymer molecules during the ejection process.[36] Larger scale coarse-grained MD simulations have been used to study the mass/size dependence of the velocity distribution of spherical solute molecules in matrix-assisted laser desorption[37] and the matrix-polymer interactions in the expanding plume.[38–40] The MD simulations reported so far, however, have been focused on the analysis of matrix-assisted ejection of individual macromolecules, with the computational systems containing either a single solute molecule[33–36] or several solute molecules at a concentration too low to involve any interactions between the molecules during the ejection process.[37–39] These conditions are justified by the fact that most of the MD simulations have been motivated by the matrix-assisted laser desorption ionization (MALDI) mass spectrometry technique,[41–43] where the goal is to optimize the conditions for the ejection of high molecular weight molecules (analytes) with minimal fragmentation. A sufficiently low analyte-to-matrix ratio is considered to be one of the key requirements for successful MALDI analysis,[43] and the interactions among the analyte molecules may indeed be insignificant under typical MALDI conditions. The concentrations of polymer molecules in MAPLE film deposition experiments, however, are much higher, typically 0.1–5 wt %, and the collective behavior of multiple polymer molecules may play an important role in defining the mechanisms of molecular ejection in MAPLE and the morphological characteristics of the deposited films.

In this paper we report the results of a comprehensive computational investigation of the processes responsible for molecular transfer in MAPLE. A coarse-grained MD model used in the simulations and parameters of the computational setup are described in Sec. II. The physical mechanisms and molecular-level picture of the molecular ejection in MAPLE, emerging from the MD simulations, are presented for a range of laser fluences and polymer concentrations in Sec. III. The parameters of the ablation plume, including the cluster size distributions, velocities of the ejected molecules and clusters, and composition of matrix-polymer clusters are given in Sec. IV. The state of the MAPLE target after one-pulse laser irradiation is analyzed in Sec. V and implications for molecular ejection in the multiple-pulse irradiation regime are discussed. Finally, in Sec. VI, we review the ramifications of the computational predictions for interpretation of experimental data and discuss promising directions for future experimental exploration, suggested by the simulation results.

II. COMPUTATIONAL MODEL

In this section we first describe the computational model that we use for simulation of the molecular ejection from frozen polymer solutions irradiated by a short laser pulse. Then we describe the computational setup and explain the choices of the irradiation parameters used in the simulations.

The laser-induced molecular ejection from a MAPLE target is described in this work by a coarse-grained molecular dynamics model combining the breathing sphere model[44] for simulation of the molecular matrix and the bead-and-spring model[45] for polymer molecules. The breathing sphere model has been actively used in investigations of laser interaction with molecular targets[37–40,44,46–48] and is described in detail elsewhere.[44,48] Briefly, the model adapts a coarse-grained representation of the molecules by spherical particles with real translational degrees of freedom, but approximate representation of the internal vibrational modes by a single internal degree of freedom. The internal degree of freedom, or breathing mode, is implemented by allowing the particles to change their sizes and is used for simulation of molecular excitation by photon absorption and vibrational relaxation of the excited molecules. In the case of UV laser irradiation, the breathing mode can be considered as the recipient of the energy released by internal conversion from electronically excited states. The parameters of a potential function attributed to the internal motion control the rate of the conversion of the internal energy of the molecules excited by the laser to the energy of translational and internal motions of the surrounding molecules.[44] In the bead-and-spring model used to describe the polymer molecules in a MAPLE target, the "beads" representing functional groups of a polymer molecule (monomers) are connected by anharmonic springs with

Downloaded 11 Oct 2007 to 128.143.68.241. Redistribution subject to AIP license or copyright, see http://jap.aip.org/jap/copyright.jsp

strengths appropriate for chemical bonding. The chains can dissociate if the local forces applied to the chemical bonds are sufficiently large.

Both the intramolecular "springs" in the bead-and-spring model and intermolecular interactions among polymer units and matrix molecules are described by a Morse potential defined as a function of the distance between the edges (surfaces) of the "breathing spheres" or polymer "beads," r_{ij}^s,

$$U(r_{ij}^s) = E_b[e^{-2\alpha(r_{ij}^s - r_0)} - 2e^{-\alpha(r_{ij}^s - r_0)}]. \quad (1)$$

Intermolecular (nonchemical) interactions among the matrix and polymer molecules are described with a set of parameters (r_0=3 Å, E_b=0.1 eV, and α=1 Å^{-1})[44]chosen to reproduce the van der Waals interaction in a typical molecular solid, with the cohesive energy of 0.6 eV, an elastic bulk modulus of ~5 GPa, and a density of 1.2 g/cm^3.[49] The parameters chosen for springs in the bead-and-spring model (r_0=1.54 Å, E_b=3.48 eV, and α=2.37 Å^{-1}) are based on the characteristics of a typical carbon-carbon bond in a polymer molecule. In particular, the value of r_0 is based on the length of the middle C–C bond in (C#)$_3$–C–CH$_2$–C# (where C# is any sp^3 carbon atom),[50] the depth of the potential well, E_b, is chosen to approximately reproduce the value of the dissociation energy of poly(methyl methacrylate) (PMMA), and α is obtained from the value of the stretching force constant for C–C bond given in Ref. 51, $d^2U/dr_{ij}^{s2}|_{r_0} = 2\alpha^2 E_b = 39$ eV/A^2.

The distance between the surfaces of two interacting molecules and/or polymer units is defined as $r_{ij}^s = |r_i - r_j| - R_i - R_j$, where r_i and r_j are the positions of the centers of the particles and R_i and R_j are their radii. Note that the radii of the breathing spheres are dynamic variables for which equations of motion are solved during the simulation. The radii of beads in the polymer bead-and-spring model are kept fixed during the simulation and are equal to the equilibrium radii of the breathing spheres, 1.40 Å. The same molecular weight of 100 Da is attributed to polymer units and matrix molecules. This weight corresponds to the weight of a PMMA monomer and is close to the weight of molecules often used as MAPLE matrices, e.g., toluene (92 Da), chloroform (118 Da), and glycerol (92 Da).

Simulations presented in this paper are performed for MAPLE targets with three concentrations of polymer molecules: 1, 3, and 6 wt %, as well as for pure matrix. Computational cell with initial dimensions of $40\times40\times60$ nm^3 (676 961 molecules in the case of pure matrix) is used in the simulations, with the polymer chains randomly and uniformly distributed in the sample. Each chain contains 100 monomer units and has the total molecular weight of 10 kDa. The total number of polymer molecules in the computational cell is 67, 202, and 381 in 1, 3, and 6 wt % samples, respectively. Periodic boundary conditions are imposed in the directions parallel to the surface, as shown in Fig. 1. These boundary conditions simulate the situation in which the laser spot diameter is much larger compared to the laser penetration depth, so that the effects of the edges of the laser beam can be neglected. At the bottom of the computational cell, a dynamic boundary condition is applied to account for nonreflecting propagation of the laser-induced pressure wave through the boundary.[52] All systems are thoroughly equilibrated in constant zero pressure simulations and cooled to zero temperature before applying laser irradiation. The size of the computational cell is then kept fixed during the simulations of laser-induced processes, thus neglecting the effect of the lateral expansion of the ablation plume during the first nanosecond of the plume expansion. A time step of 5 fs is used in the integration of the MD equations of motion in simulations performed for pure matrix targets, whereas a smaller time step of 2 fs is used if polymer chains are present. The molecular trajectories are followed at least up to 1 ns and longer in some of the simulations.

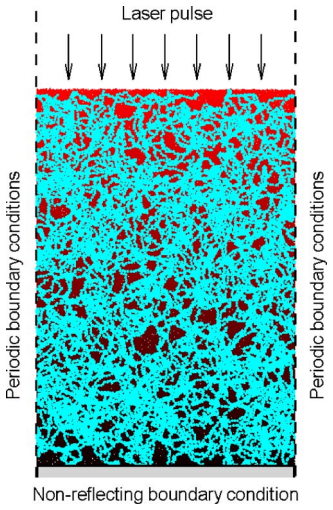

FIG. 1. (Color online) Schematic sketch of the simulation setup shown for the initial MAPLE target containing 3 wt % of polymer chains. The polymer chains are shown in blue and are superimposed on top of the image of matrix molecules shown in the background. The color of matrix molecules schematically shows the energy density deposition by the laser pulse.

The laser irradiation is simulated by deposition of quanta of energy equal to the photon energy into the kinetic energy of internal (breathing) motion of molecules that are randomly chosen during the laser pulse duration. Irradiation at a wavelength of 337 nm (photon energy of 3.68 eV) is simulated in this study. The total number of photons entering the model during the laser pulse is determined by the laser fluence. The probability of a molecule to be excited is modulated by Lambert-Beer's law to reproduce the exponential attenuation of the laser light with depth, as schematically shown by color in Fig. 1. The absorption by polymer molecules is neglected in this study and the effective penetration depth is increased with increasing concentration of polymer molecular in the MAPLE target. A total of 21 simulations are performed for MAPLE targets with three polymer concentrations, with seven laser fluences of 3, 4, 5, 6, 7, 8, and 9 mJ/cm^2 used with each target. The laser fluences are chosen to cover the range from below the ablation threshold (3.5 mJ/cm^2 for pure matrix) up to more than twice the ablation threshold.

The laser pulse duration of 50 ps and optical penetration depth in pure matrix of 50 nm are chosen to reproduce the conditions of thermal confinement[43,46–48,53] characteristic of the majority of experimental studies of MAPLE. In this irra-

Downloaded 11 Oct 2007 to 128.143.68.241. Redistribution subject to AIP license or copyright, see http://jap.aip.org/jap/copyright.jsp

diation regime, the heat conduction does not contribute to the energy redistribution during the laser pulse and the thermal energy is largely confined within the absorbing region. The condition for the thermal confinement of the deposited laser energy can be expressed as $\tau_p < \tau_{th} = (L_p^2)/(AD_T)$, where τ_p is the laser pulse duration, D_T is the thermal diffusivity of the target material, L_p is the laser penetration depth, and A is a constant defined by the geometry of the absorbing region. Thermal diffusivity is evaluated for the model material (pure matrix) by performing a MD simulation of heat diffusion from a constant temperature layer located in the middle of a large computational cell initially equilibrated at a lower temperature. Fitting the results of the MD simulation to the analytical solution of the heat diffusion equation gives $D_T = 3.6 \times 10^{-7}$ m^2/s. If we assume one-dimensional heat diffusion from the absorbing region to the bulk of the target and define the thermal diffusion time τ_{th} as time required for half of the thermal energy initially evenly distributed within a surface region of size L_p to transfer to the deeper parts of the target, the constant A can be taken as unity. The thermal diffusion time for $L_p = 50$ nm can be then estimated as $\tau_{th} \approx 7$ ns. This time is significantly longer than the pulse duration, $\tau_p = 50$ ps, and the condition for the thermal confinement is satisfied. At the same time, the rate of the laser energy deposition is sufficiently low to allow for the mechanical relaxation (expansion) of the absorption region of the target during the laser pulse and the condition of the inertial stress confinement[43,46,48,53,54] is not achieved. The condition for the stress confinement can be expressed as $\tau_p < \tau_s \sim L_p/C_s$, where C_s is the speed of sound in the target material, measured to be 2300 m/s for the model system (pure matrix). Thus, the characteristic time of the mechanical relaxation of the absorbing volume, τ_s, can be estimated to be around 20 ps and the condition for the stress confinement is not satisfied in the simulations.

The conditions of thermal confinement, but not stress confinement, are also characteristic for the majority of MAPLE experiments performed with nanosecond laser pulses. For example, for MAPLE experiments reported in Refs. 18, 20, 30, and 31 and performed with toluene matrix [$C_s = 1306$ m/s,[55] $D_T = 0.885 \times 10^{-7}$ m^2/s at 25 °C (Ref. 50)], laser pulse duration of 25 ns, and laser penetration depth of 4 μm at 248 nm,[56,57] the characteristic times of the mechanical and thermal relaxations of the absorbing volume can be estimated as $\tau_s \approx 3$ ns and $\tau_{th} \approx 181$ μs, respectively.[18] These estimations firmly place the conditions of the experiments in the regime of thermal confinement, $\tau_s < \tau_p < \tau_{th}$. Thus, although the length and time scales of the simulations are very different from the ones in a typical MAPLE experiment, the fact that in the simulations and experiments the MAPLE process takes place under similar physical conditions (the same physical regime of thermal confinement) suggests that the ejection mechanisms revealed in the simulations are also at work in experiments, albeit at much larger time and length scales. Nevertheless, we would like to emphasize that the goal of this computational study is not to reproduce quantitatively the behavior of a particular molecular system, but to investigate the general characteristics of the ablation process for low-concentration polymer solutions in the thermal confinement regime. The natural limits of the applicability of the model are defined by the conditions for the onset of multiphoton absorption, photochemical fragmentation, ionization, and plasma formation.

III. MECHANISMS OF MOLECULAR EJECTION IN MAPLE

In this section the mechanisms of molecular ejection in MAPLE are discussed with a focus on the analysis of the effect of polymer molecules on the dynamics of the ablation process. A visual picture of the initial processes of the explosive matrix disintegration and collective ejection of a surface region of the irradiated target is shown in Fig. 2 for four simulations performed at the same laser fluence of 8 mJ/cm^2 for pure matrix and three MAPLE targets with polymer concentrations of 1, 3, and 6 wt %.

The ablation mechanisms and parameters of the ablation plume for one-component molecular systems (pure matrix) have been discussed in detail earlier.[46–48] A typical dynamics of the ablation process in a one-component system is illustrated in Fig. 2(a), where snapshots from a simulation performed for a target containing no polymer molecules are shown. The ablation starts from a homogeneous expansion of a significant part of the surface region overheated above the limit of its thermodynamic stability[58,59] and proceeds through the formation of a foamy transient structure of interconnected liquid regions[47] that subsequently decomposes into a mixture of liquid droplets and gas-phase matrix molecules.

In the ablation of MAPLE target, the presence of polymer molecules does not radically alter the general picture of the ablation process, with the explosive disintegration and expansion of the overheated matrix driving the ejection process and entraining the polymer molecules along, Figs. 2(b)–2(d). The presence of the polymer molecules (shown in blue in the snapshots), however, does have significant implications on the dynamics of the ablation process and quantitative parameters of the ejected plume. Although the polymer molecules are randomly oriented in the initial target, Fig. 1, they have a clear tendency to extend along the flow in the ablation plume and to thread through the liquid regions, Figs. 2(b)–2(d). The decomposition of the transient foamy liquid structure is hampered by the necessity to pull out and, at higher polymer concentrations, to disentangle the polymer chains (no breakdown of polymer chains has been observed in any of the simulations discussed in this paper). As a result, while in the simulation performed for pure matrix the liquid regions emerging from the "phase explosion" quickly transform into spherical droplets as soon as they separate from the target, Fig. 2(a), the presence of polymer chains facilitates the formation of complex matrix-polymer liquid structures elongated in the direction of the ablation plume expansion and stabilized by the presence of polymer molecules, Figs. 2(c) and 2(d).

A broad qualitative picture of the fluence and polymer concentration dependence of the molecular ejection process in MAPLE can be gained from Fig. 3, where snapshots from the simulations performed with initial polymer concentrations of 1, 3, and 6 wt % are shown for seven laser fluences, from 3 to 9 mJ/cm^2, and for the same time of 400 ps after

Downloaded 11 Oct 2007 to 128.143.68.241. Redistribution subject to AIP license or copyright, see http://jap.aip.org/jap/copyright.jsp

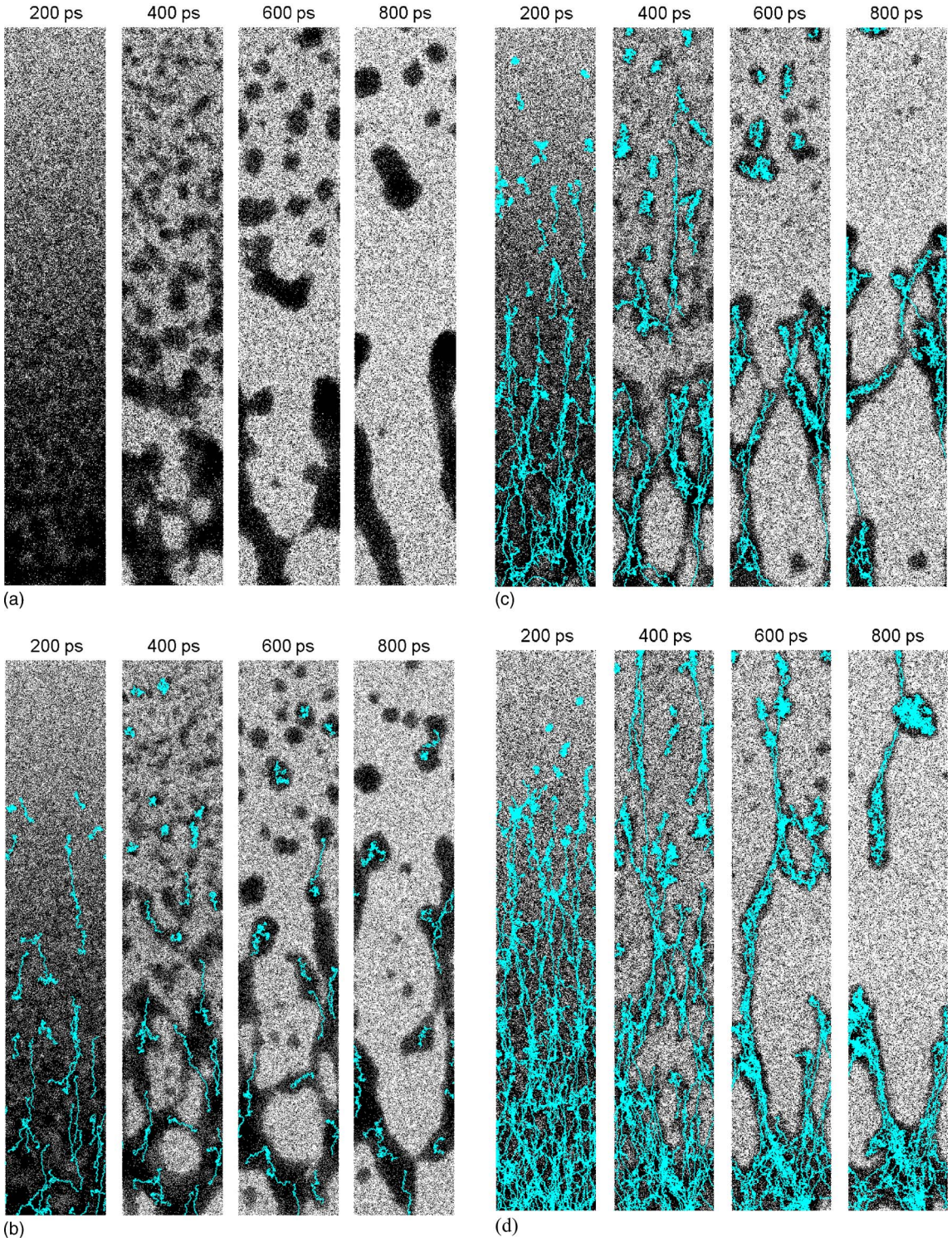

FIG. 2. (Color online) Snapshots from simulations of laser ablation performed for pure matrix (a) and MAPLE targets with polymer concentrations of 1 (b), 3 (c) and 6 wt % (d). The same fluence of 8 mJ/cm^2 is used in all four simulations. The polymer chains are shown in blue and are superimposed on top of the image of matrix molecules shown in the background.

the beginning of the 50 ps laser pulse. In all three series of simulations, there is a clear change in the mechanism of molecular ejection as laser fluence increases from 3 to 4 mJ/cm^2. At 3 mJ/cm^2, the targets undergo some expansion/swelling that is more pronounced for targets with lower polymer concentrations (the initial positions of the surface before the irradiation are marked by red dashed lines in the first frames of each series shown in Fig. 3). The molecular ejection at this fluence is limited to thermal evaporation of individual matrix molecules. At 4 mJ/cm^2, we observe a transition to the ablation regime, when active collective motion in the surface region of the irradiated target is induced by an explosive internal release of the matrix vapor. The onset of the explosive boiling is characterized by prompt ejection of small clusters from the topmost layer of the target, as well as much slower motion of large liquid regions

Downloaded 11 Oct 2007 to 128.143.68.241. Redistribution subject to AIP license or copyright, see http://jap.aip.org/jap/copyright.jsp

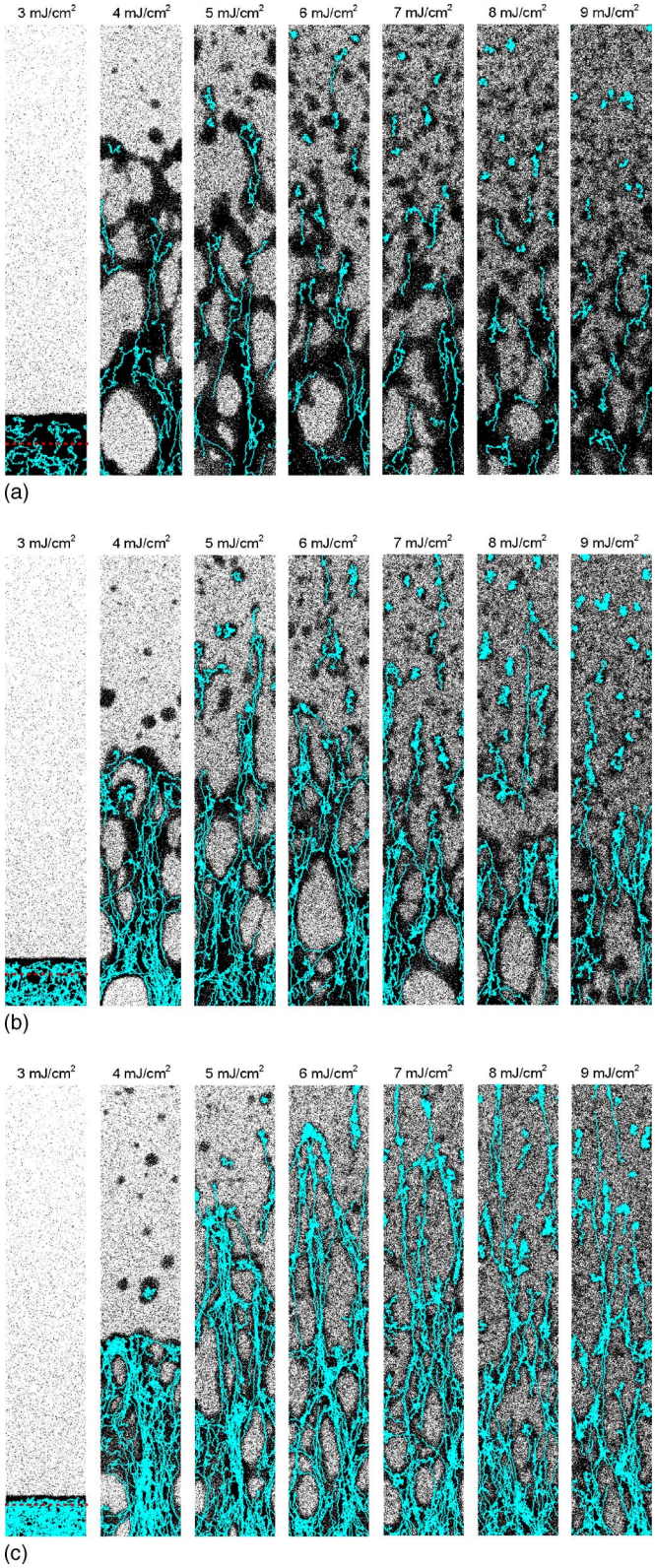

FIG. 3. (Color online) Snapshots taken at 400 ps after the beginning of the laser pulse in simulations of MAPLE. Laser fluences are shown above the snapshots. Polymer concentrations in MAPLE targets are 1, 3, and 6 wt % in (a), (b), and (c), respectively. The polymer chains are shown in blue and are superimposed on top of the image of matrix molecules shown in the background. The initial positions of the target surface before the laser irradiation are shown in the left frames by red dashed lines.

that can eventually result in the ejection of large elongated matrix-polymer structures (see Secs. IV and V). Further increase of the laser fluence results is a more violent phase explosion of the overheated material, with more numerous polymer-matrix clusters ejected.

The existence of a well-defined threshold fluence separating the desorption and ablation regimes of molecular ejection can be related to the sharp transition from a metastable superheated liquid to a two-phase mixture of liquid and vapor (explosive boiling or phase explosion) at a temperature of approximately 90% of the critical temperature, predicted by the classical nucleation theory[58,59] and confirmed in simulations.[60] Following the method applied in Ref. 60 to a system of Ar atoms, we find the threshold temperature for the onset of explosive boiling, T^*, to be 1060 K for the pure matrix system represented by the breathing sphere model. This temperature is determined in a constant pressure MD simulation performed for a system consisting of 6912 matrix molecules. Starting from a metastable liquid equilibrated at 900 K, the temperature is increased with a rate decreasing from 0.1 to 0.025 K/ps as the temperature is approaching the threshold. The threshold temperature T^* manifests itself by the onset of the phase separation and a sharp increase of the volume of the system. At low polymer concentrations, the threshold temperature T^* has a weak dependence on the polymer concentration, with only 4.7% increase predicted for a system containing 16 wt % of polymer chains (134 142 matrix molecules and 256 polymer chains). Therefore, we will use the value of the threshold temperature T^* determined for pure matrix in the discussion of all the MAPLE simulations.

The effect of the presence of polymers on the characteristics of the ablation process becomes stronger with increasing polymer concentration. At low polymer concentration, Fig. 3(a), the chains are not heavily entangled and the presence of individual polymer chains in the expanding overheated matrix has a relatively weak effect on the overall dynamics of the ablation plume formation. As the polymer concentration increases, the chains become more entangled and the expansion and disintegration of the transient foamy liquid-vapor mixture result in multiple chains being pulled out from the liquid regions, resisting the disintegration process, Fig. 3(b). The effect of the entanglement of the polymer chains on the ablation process manifests itself even more dramatically in Fig. 3(c), where the entanglement of the polymer chains leads to the formation of intricate elongated structures that, in some of the simulations, extend throughout the region shown in the snapshots. While the expanding liquid structures eventually disintegrate into individual liquid regions, Fig. 2(d), the elongated shapes characteristic for these regions are very different from the spherical droplets observed in simulations of laser ablation of pure matrix targets. The elongated structures can be stabilized by evaporative cooling in the expanding plume and can reach the substrate in MAPLE film deposition. Indeed, extended "nanofiber" or "necklace" polymer surface features have been observed in SEM images of PMMA films deposited in MAPLE,[18,30,31] as well as in films fabricated by IR laser ablation of poly(vinyl chloride) (PVC) involving a partial thermal decomposition of the target material into volatile species.[61] Some of the transient liquid structures do not sepa-

Downloaded 11 Oct 2007 to 128.143.68.241. Redistribution subject to AIP license or copyright, see http://jap.aip.org/jap/copyright.jsp

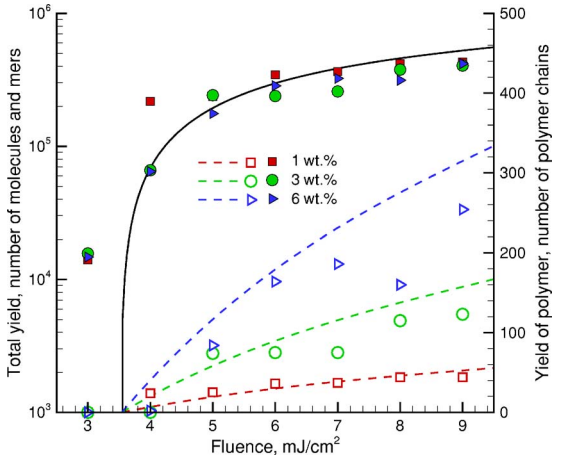

FIG. 4. (Color online) Total yield of matrix molecules and polymer units (closed symbols) and yield of polymer chains (open symbols) as function of laser fluence in simulations performed for MAPLE targets with polymer concentrations of 1 wt % (red squares), 3 wt % (green circles), and 6 wt % (blue triangles). The black solid line represents prediction of the ablation model, Eq. (2), where the critical energy is assumed to be equal to the cohesive energy of the matrix material, $E^*=0.6$ eV/molecule, and the laser penetration depth of pure matrix, $L_p=50$ nm, is used. The dashed lines correspond to a percentage of the solid line that equals the amount of polymer in the original target.

rate from the target or can be redeposited within or outside the laser spot, resulting in the formation of complex surface morphology. Experimentally, the generation of extended nanofibers[62–64] and surface swelling and foaming[65–68] have been reported for polymer and biopolymer targets subjected to short pulse laser irradiation. Recently, a significant macroscopic swelling has been observed for a MAPLE target with 10 wt % PMMA loading and toluene as a matrix.[69] A more detailed discussion of the characteristics of the ablation plume and the parameters of the droplets ejected and deposited in MAPLE is given in Sec. IV, whereas target surface modification by the laser pulse is considered in Sec. V.

The qualitative conclusions on the effect of the polymer molecules on the mechanisms of laser ablation of MAPLE targets, based on the visual inspection of the snapshots from the simulations, Figs. 2 and 3 can be supported by a quantitative analysis of the dependences of the total yield of ejected molecules on laser fluence, shown in Fig. 4 for MAPLE targets with three polymer concentrations. Most data points in Fig. 4 are calculated at 1 ns after the beginning of the 50 ps laser pulse, with several exceptions made for the simulations in which a delayed separation of large liquid regions from the target has been observed. In particular, the yield is shown for 1.5 ns in the simulation performed at a fluence and polymer concentration of ($F=6$ mJ/cm^2; $C=1$ wt %), for 1.3 ns in ($F=4$ mJ/cm^2; $C=1$ wt %) and ($F=6$ mJ/cm^2; $C=6$ wt %), for 1.2 ns in ($F=7$ mJ/cm^2; $C=6$ wt %), and for 1.1 ns in four other simulations. While evaporation during the extra several hundreds of picosecond would make relatively minor contributions to the total yields in the simulations run for 1 ns (up to several thousands of molecules), the contribution from the delayed separation of large liquid regions is much more significant (tens of thousands of molecules). Therefore, some misalignment of times for which the data points are shown in Fig. 4 is making this plot more representative of the total amount of material ejected from the target during the first 1–1.5 ns. The polymer molecules are only ejected as parts of matrix-polymer clusters, with no additional polymer ejection taking place at the evaporation stage. Therefore, the yield of polymer chains shown in Fig. 4 for 1 ns or the time of the separation of the last liquid region from the target is the final total number of polymer chains ejected from the target.

The characteristic feature of the fluence dependences of the total yield observed at all three polymer concentrations is a sharp increase of the amount of ejected material as the fluence increases from 3 to 4 mJ/cm^2. The increase in the total yield is by almost an order of magnitude, from 14 082 to 115 595 molecules, in simulations performed for a MAPLE target with polymer concentration of 1 wt %, and is somewhat smaller, from 15 699 to 66 010 molecules and from 14 760 to 64 598 molecules in simulations performed for MAPLE targets with higher polymer concentrations of 3 and 6 wt %. In earlier simulations performed for one-component molecular system (pure matrix), a similar sharp increase in the total yield has been observed and attributed to the transition from the thermally activated desorption of individual molecules from the surface to a collective molecular ejection of an overheated region of the target (ablation).[46,48,70,71] The increase of the total yield at the threshold for the ablation onset in the case of the pure matrix, however, was more dramatic, by more than an order of magnitude, suggesting that the presence of the polymer molecules in MAPLE targets is having an impeding effect on the ablation process.

Similarly to the earlier MD simulations[44,46,48,70,71] and experiments on laser ablation of molecular substrates,[72] polymers,[73,74] and biological tissue,[53] we attempt to describe the amount of material ejected from MAPLE targets in the ablation regime by a model in which the ablation depth is assumed to follow the laser energy deposition and all material that absorbs an energy density higher than a critical energy density, E^*, is ablated. With an exponential decay of the laser intensity given by Beer's law, the number of molecules ejected from unit surface area at laser fluence exceeding the threshold for the ablation onset is

$$Y = nL_p \ln\left[\frac{F}{L_p(E^* - CT_0)}\right], \tag{2}$$

where n is the molecular number density, L_p is the laser penetration depth, C is the heat capacity, T_0 the initial temperature of the target, and F the absorbed laser fluence. In the earlier simulations performed for pure matrix,[46,71] the value of the critical energy density equal to the cohesive energy of the molecular solid, 0.6 eV/molecule, was found to provide the best fit of the ablation yield in the regime of thermal confinement. The prediction of the ablation model with the same critical energy density, $E^*=0.6$ eV/molecule, laser penetration depth for pure matrix, $L_p=50$ nm, and zero initial temperature of the target, $T_0=0$ K, is shown by the black solid line in Fig. 4.

While the overall character of the yield versus fluence dependence above the threshold fluence $F_{th}=L_p(E^*-CT_0)=3.54$ mJ/cm^2 is captured by the ablation model, the in-

Downloaded 11 Oct 2007 to 128.143.68.241. Redistribution subject to AIP license or copyright, see http://jap.aip.org/jap/copyright.jsp

crease of the yield with fluence is weaker as compared to the predictions of the model and there are significant deviations of the simulation results from the model at high laser fluences. Despite a large scatter of the data points related to the statistical nature of the contribution from the separation of large liquid regions to the ablation yield, the tendency of the decreasing yield with increasing polymer concentration can be observed by comparing the results obtained for target with polymer concentration of 1 wt % with the ones having higher polymer concentrations. The deviation of the ablation yield from the prediction of Eq. (2) at high laser fluences is significantly larger than in the case of pure matrix[46,71] and can only partially be explained by the increase of the effective penetration depth with increasing polymer concentration (from 50.5 nm at 1 wt % to 51.5 nm at 3 wt %, and to 53 nm at 6 wt %). An important factor defining the ablation yield is the resistance of the polymer molecules to the matrix disintegration. The entanglement of the polymer chains at higher polymer concentrations increases the effective cohesion and viscosity of the target material, thus hampering the ejection process.

The yield of polymer molecules is shown in Fig. 4 by open symbols. As discussed above, not a single polymer molecule has been ejected in any of the simulations performed in the desorption regime, at 3 mJ/cm^2. The fluence dependence of the number of polymer molecules in the ablation regime can be related to the prediction of the ablation model, Eq. (2), shown by dashed lines under an assumption of stoichiometric ejection of matrix and polymer molecules. Similarly to the total yield, the deviation of the simulation results from the model increases with increasing polymer concentration and laser fluence. The analysis of the plume composition indicates that the polymer concentration in the plume tends to be lower than in the original target, with more pronounced nonstoichiometric ejection observed at higher polymer concentrations. Moreover, the yield of polymer molecules shown in Fig. 4 is final, with no further ejection of polymer chains expected at longer times. At the same time, the evaporation of matrix molecules remains relatively active at the end of the simulations (see Sec. IV), suggesting that the nonstoichiometric composition of the ablation plume will become more pronounced with time. As a result, the surface region of the irradiated target becomes depleted of matrix molecules, as discussed in Sec. V. Similar changes in the composition of the surface region of the target take place in the desorption regime, where molecular ejection is limited to the evaporation of matrix molecules. The sharp threshold transition from the desorption of matrix molecules to the collective coejection of matrix and polymer molecules, predicted in the simulations, may be related to recent experimental observations of the transition from a wavelength-selective desorption of one of the components of a binary molecular mixture to codesorption of the two components at higher fluences.[75,76]

The fluence dependence of the number of individual matrix molecules ejected during the first nanosecond of the simulations is shown in Fig. 5. In contrast to the total yield, the yield of matrix monomers does not exhibit the sharp increase at the ablation threshold, between 3 and 4 mJ/cm^2.

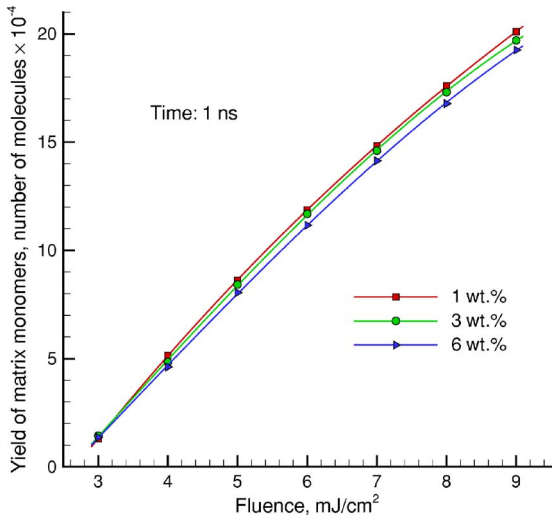

FIG. 5. (Color online) Yield of individual matrix molecules as a function of laser fluence in simulations performed for MAPLE targets with polymer concentrations of 1 wt % (red squares), 3 wt % (green circles), and 6 wt % (blue triangles). The data are for 1 ns after the beginning of the laser pulse. The lines are guides to the eye.

Moreover, the ablation threshold cannot be identified from the fluence dependence of the monomer yield, which shows a monotonous increase in the whole range of laser fluences used in the simulations. This observation is consistent with the results of earlier MD simulations performed for pure matrix,[40,46,48,70,71] as well as with the mass spectrometry data showing an apparent absence of the real physical threshold behavior in the fluence dependence of the number of individual neutral matrix molecules (monomers) postionized by a second laser and detected in MALDI experiments.[43,77,78] These results indicate that the yield of monomers is not sensitive to the transition from the desorption to the volume ablation ejection regime.

A clear tendency of the yield of monomers to decrease with increasing polymer concentration, Fig. 5, can be related to the impeding effect of polymers on the explosive decomposition of the overheated matrix. For the same laser fluence, ablation in a target with a higher polymer concentration results in the ejection of larger liquid droplets stabilized by the presence of polymer chains. The larger droplets tend to have higher internal temperatures[47] and a slower rate of evaporative cooling, resulting in the reduction of the fraction of vapor in the ablation plume at a given time in the ablation process.

IV. DYNAMICS OF THE EJECTION PROCESS AND PARAMETERS OF THE PLUME

The time evolution of the molecular ejection process in MAPLE is illustrated in Figs. 6 and 7 for a simulation performed for a target with polymer concentration of 6 wt % irradiated at a fluence of 8 mJ/cm^2. The long duration of this simulation, 2.5 ns, allows us to study not only the dynamics of material disintegration and prompt ejection, but also longer-term processes in the expanding plume and at the irradiated target.

Downloaded 11 Oct 2007 to 128.143.68.241. Redistribution subject to AIP license or copyright, see http://jap.aip.org/jap/copyright.jsp

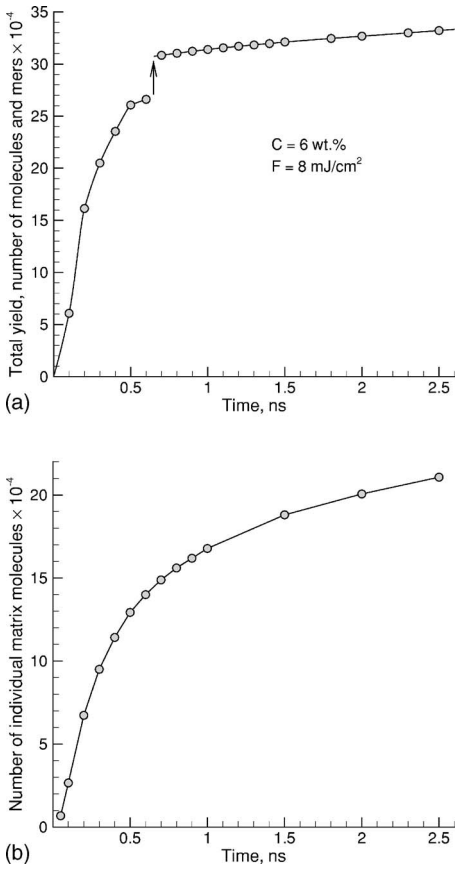

FIG. 6. Evolution of the total molecular yield (a) and the yield of matrix monomers (b) in a simulation performed with a fluence of 8 mJ/cm^2 and polymer concentration of 6 wt %. The total yield is defined as the number of ejected matrix molecules and polymer units (mers). The arrow in (a) corresponds to the separation of a large cluster, shown in the left inset in Fig. 7(a), from the target at ~650 ps.

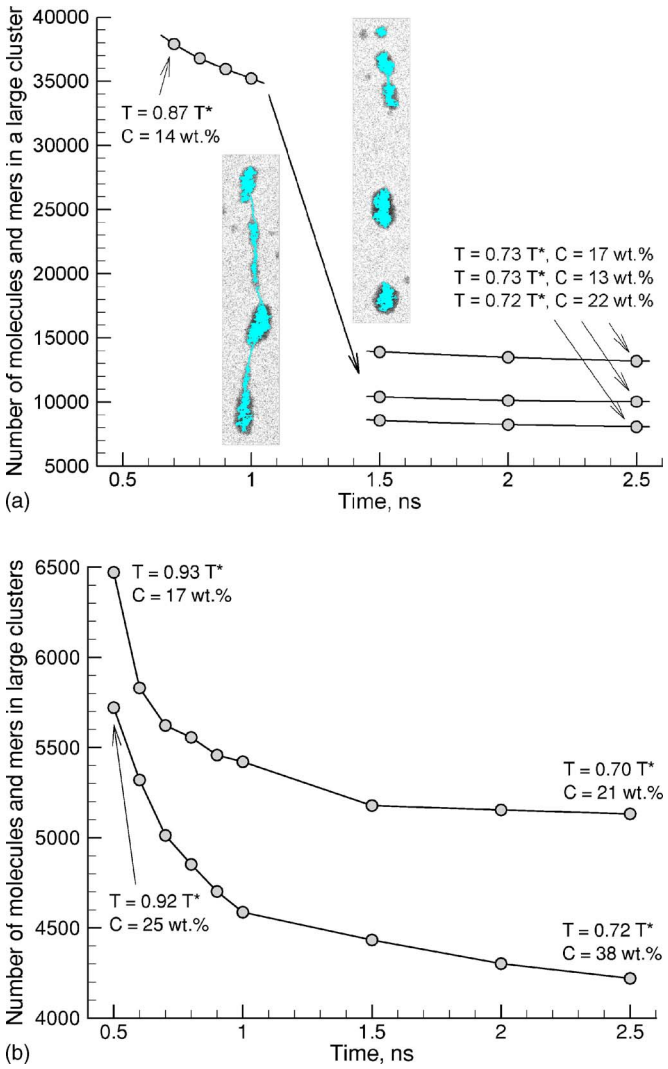

FIG. 7. (Color online) Evolution of the sizes of three largest clusters ejected in a simulation performed at a fluence of 8 mJ/cm^2 and polymer concentration of 6 wt %. Internal temperatures and polymer concentrations in the clusters at early times of (a) 700 and (b) 500 ps, as well as at the end of the simulation, 2.5 ns, are shown in the figure. The temperature values are expressed through the threshold temperature for the phase explosion, T^*. In (a), the elongated cluster disintegrates into three large and one smaller clusters at ~1.2 ns, as illustrated by insets showing the cluster at 1 and 1.3 ns.

The total yield plotted in Fig. 6(a) includes all monomers, liquid droplets, and small molecular clusters that are ejected from the target at a given time. Several stages can be distinguished in the material ejection process in this simulation. First, the initial explosive decomposition of the overheated target (see Sec. III) results in a prompt ejection of a large fraction, 78%, of the total yield observed at 2.5 ns during the first 500 ps of the simulation. The increase of the total yield slows down after 500 ps, but an additional abrupt increase of the yield takes place at ~650 ps. This increase, by ~14% of the total yield at 2.5 ns, corresponds to the separation of the largest molecular droplet ejected in this simulation from the surface of the target. A part of this elongated droplet can be seen in the upper part of the rightmost frame shown in Fig. 2(d). The following slow monotonous increase of the total yield corresponds to the evaporation of the matrix molecules from the target. The evaporation during the last 1.8 ns of the 2.5 ns simulation accounts for ~7% of the total yield. The evaporation slows down as the temperature of the surface decreases due to the heat conduction to the bulk of the target that occurs on the time scale of the simulation ($\tau_{th} \approx 7$ ns is estimated in Sec. II), as well as due to the evaporative cooling. The evaporation continues to contribute to the total yield at the end of the simulation and one can expect to see a gradual decrease of the evaporation rate within the following tens of nanoseconds. Note that for typical experimental conditions in MAPLE and laser ablation of molecular systems, the laser penetration depth is typically much larger than 50 nm used in the simulations, leading to a much slower cooling process and a longer-term molecular desorption. For example, in recent IR laser resonant desorption time-of-flight mass spectrometry experiments performed for a range of molecular systems, the desorption times were shown to extend up to several hundreds of microseconds[79] and, for some systems, even up to milliseconds.[80] The latter abnormally long desorption time has been attributed to the long penetration depth and low thermal conductivity of the molecular system.

Two stages of the ejection process discussed above for the total yield can be also identified in the time dependence of the number of monomers shown in Fig. 6(b). The initial raise in the number of monomers during the first 500 ps of

Downloaded 11 Oct 2007 to 128.143.68.241. Redistribution subject to AIP license or copyright, see http://jap.aip.org/jap/copyright.jsp

the simulation corresponds to the explosive release of the vapor during the decomposition of the overheated target. This is followed by a slower increase due to the evaporation from the target and liquid droplets, as well as thermal decomposition of small molecular clusters. The evaporation slows down as the temperatures of the droplets and target surface are decreasing, but it still remains noticeable at 2.5 ns after the laser pulse.

The extent to which the evaporation affects the sizes of the matrix-polymer droplets can be seen from Fig. 7, where the evolution of the three largest clusters ejected in the simulation discussed above is shown. The largest cluster separates from the target at ~650 ps, as reflected by the jump in the total yield in Fig. 6(a). This cluster has an extended elongated shape and it disintegrates into three large and one smaller fragments between 1 and 1.3 ns. The snapshots of the cluster before and after the disintegration are shown in the insets in Fig. 7(a). The decrease of the size of the cluster(s) before and after the disintegration reflects the evaporation process that clearly slows down by the time of 2.5 ns. The decrease of the rate of evaporation can be related to the evaporative cooling of the cluster(s), which leads to the decrease of the temperature from 87 to 72–73% of the threshold temperature for the phase explosion, T^*, defined in Sec. III.

Similarly, two large clusters for which the size evolution is shown in Fig. 7(b), are emerging from the phase explosion at 500 ps with temperatures as high as $0.92T^*$ and $0.93T^*$, but cool down to temperatures of $0.70T^*$ and $0.72T^*$ by the time of 2.5 ns. The rate of evaporative cooling has strong temperature dependence, with the most active cooling occurring within the first nanosecond after the laser pulse. Importantly, the quickly decreasing rates of evaporation of the ejected clusters suggest that the sizes and compositions of the clusters observed at 2.5 ns are close to the ones to be expected at the time when they reach the substrate in MAPLE deposition of polymer films.

Since in all simulations the polymer molecules are ejected only as parts of large matrix-polymer droplets/clusters that do not have enough thermal energy to evaporate during the flight to the substrate, one can expect that the growth of polymer films in MAPLE proceeds mainly through the deposition of matrix-polymer clusters. This observation goes against the notion of the ejection and transport of individual polymer molecules in MAPLE,[1–3] and provides a hint for explaining the observed surface roughness in the experimental AFM and SEM images.[11,14,18,23–25,27–30] In particular, the deposition and subsequent evaporation of a significant amount of volatile matrix can be related to the formation of wrinkled surface features observed in recent MAPLE experiments.[18,30] The connections between the ejection of large matrix-polymer droplets in MAPLE, predicted in the simulations, and the resulting morphological characteristics of the growing films, observed in experiments, are summarized in Sec. VI.

The collective and explosive character of the processes responsible for the initial emission and acceleration of the ablation plume in MAPLE results in a strongly forward peaked ejection, with high flow velocities in the direction

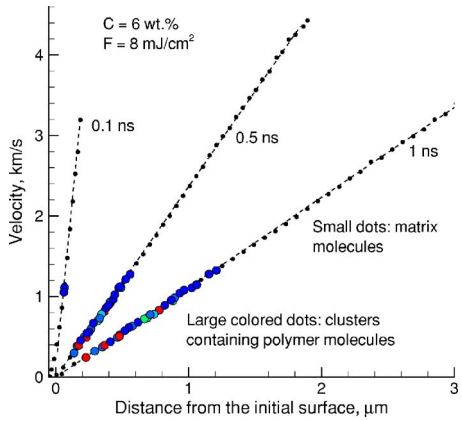

FIG. 8. (Color online) Flow velocities in the direction normal to the surface shown for the ejected matrix molecules and clusters containing polymer molecules as a function of the distance from the initial surface of the target. The velocities are plotted for three different times, 0.1, 0.5, and 1 ns, during the simulation performed with a fluence of 8 mJ/cm^2 and polymer concentration of 6 wt %. The small black dots show the average velocities of the matrix monomers. The large colored circles show the velocities of individual molecular clusters containing polymer molecules, with color indicating the number of polymer chains in the clusters, from red color used for clusters containing more than ten polymer chains to blue color used for clusters with only one chain.

normal to the surface of the target. The flow velocities of matrix molecules and clusters containing polymer molecules are shown in Fig. 8 as a function of the distance from the initial surface. As early as 100 ps after the beginning of the laser pulse, we observe the ejection of matrix molecules with the maximum velocity as high as 3.2 km/s. As the ablation plume expands, some of the matrix molecules experience additional acceleration up to 4.6 km/s. At the same time, most of the clusters containing polymer molecules have the flow velocities in hundreds of m/s, with only several relatively small clusters moving faster than 1 km/s. All plume components, including the largest droplets, have the identical linear dependences of the flow velocity on the distance from the surface, characteristic of the free-expansion model. This suggests that the clusters of different sizes acquire their velocities at the early stages of the ablation process and move along with the matrix molecules with the same velocities.

The forwarded ejection of different plume components can be illustrated by angular distributions of molecules and clusters of different sizes shown in Fig. 9 for two simulations performed at the same laser fluence of 8 mJ/cm^2 for a pure matrix target and a MAPLE target with 6 wt % polymer loading. While both individual matrix molecules and clusters have forward-picked angular distributions, the clusters of higher mass exhibit a higher degree of forward peaking. This observation can be related to the origin of the axial (normal to the surface) and radial (parallel to the surface) velocity components of the ejected species. The axial velocities of molecules and clusters are largely defined by the collective ejection process driven by the explosive decomposition of the overheated matrix and have a weak mass dependence. Indeed, the axial velocity of a molecule or a cluster depends on its location in the plume, Fig. 8, which, in turn, is related to the dynamics of the ablation plume formation resulting in a spatial segregation of clusters of different sizes in the ex-

Downloaded 11 Oct 2007 to 128.143.68.241. Redistribution subject to AIP license or copyright, see http://jap.aip.org/jap/copyright.jsp

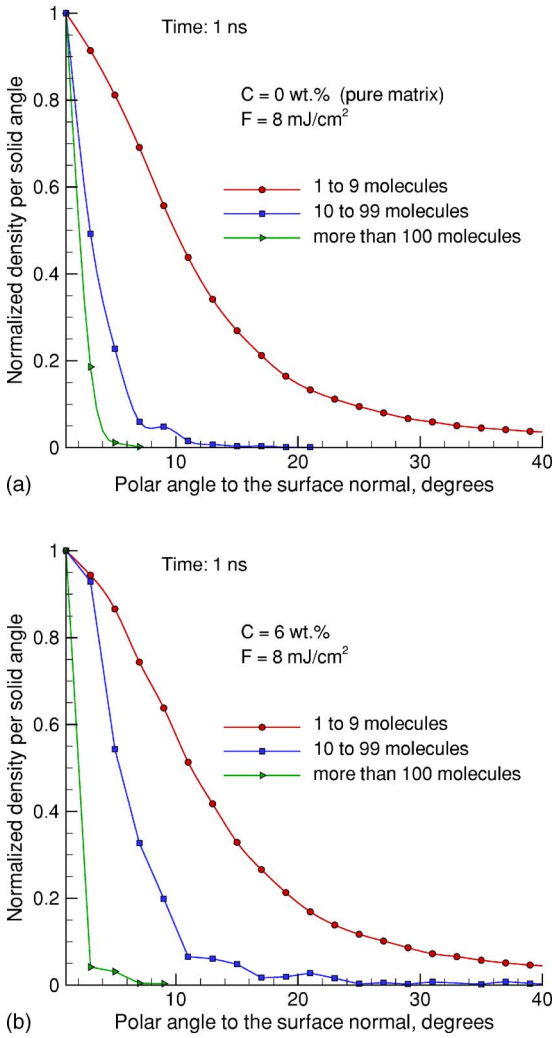

FIG. 9. (Color online) Angular distributions of the ejected molecules and clusters of different sizes in simulations performed at a fluence of 8 mJ/cm^2 for (a) pure matrix and (b) MAPLE target with a polymer concentration of 6 wt %. To provide a statistically adequate representation of the distributions for large clusters, the distributions are plotted for groups of clusters, as indicated in the legends. The densities of molecules/clusters per solid angle are normalized to the maximum of the distributions. The distributions are shown for 1 ns after the beginning of the laser pulse.

panding plume.[47] The radial velocity components of molecules and small clusters, on the other hand, are largely defined by local thermalization in the plume, resulting in narrower "thermal" distributions of the radial velocities for larger/heavier clusters. Thus, the clusters of higher mass exhibit a larger disparity between the axial and radial velocity components, resulting in a sharper forward peaking of the angular distributions, Fig. 9. The thermalization may be incomplete for the largest droplets, in which case the radial velocity components also reflect the dynamics of the ejection process. Somewhat broader angular distributions of small clusters and monomers observed in Fig. 9 for MAPLE target can be attributed to the restraining effect of the entangled polymer molecules on the ejection process (see Sec. III), leading to the decrease of the axial components of the ejection velocities as compared to a pure matrix target irradiated at the same laser fluence.

Experimentally, highly forward peaked angular distributions of ejected molecules have been observed in laser ablation of molecular solids, e.g., Refs. 81 and 82, whereas the stronger focusing of clusters toward the surface normal can be related to the weak mass dependence of the ejection velocities and higher degree of forward peaking observed for heavier analyte molecules in MALDI.[82–86] Similarly to the matrix-polymer clusters in MAPLE, the large biomolecules in MALDI are entrained into the plume of smaller matrix molecules and move along with the matrix molecules with the same flow velocities in the direction normal to the surface of the target.[37,40]

In all simulations performed above the ablation threshold, the ejected plume consists of a mixture of individual matrix molecules, small matrix clusters, and larger clusters/droplets composed of both matrix molecules and polymer chains. The results of the simulations suggest that the polymer molecules are ejected and transferred to the substrate in MAPLE experiments as parts of large molecular clusters. The size distribution of the ejected clusters, therefore, is an important characteristic of the MAPLE process as it defines the homogeneity and morphology of the deposited polymer films. Typical cluster size distributions are shown in Fig. 10 for simulations performed at the same laser fluence of 8 mJ/cm^2 and polymer concentrations of 0, 1, 3, and 6 wt %. The yield is normalized to the number of matrix monomers and is calculated at 1 ns after the beginning of the laser pulse. For all concentrations, we observe cluster-size distributions that can be relatively well described by a power law of the form $Y(N) \propto N^{-t}$ with exponents different for low- and high-mass clusters (N is the size of a cluster that can be defined as the total mass or the number of matrix molecules and polymer units/mers in the cluster). The steep size dependence observed for small clusters (up to 20 molecules) corresponds to the power-law exponents ($-t$) in the range from −3.69 to −3.59. The decay is much slower in the high-mass region of the distributions that can be described by a power law with two to three times larger exponent, from −1.43 to −1.35.

In all simulations performed in this work at laser fluences above the ablation threshold, we observe bimodal power-law cluster size distributions similar to the ones presented in Fig. 10. The values of the power-law exponents are given in Fig. 11 for three polymer concentrations and fluences ranging from 4 to 9 mJ/cm^2. The exponents for small clusters are in the range from −4.1 to −3.5, whereas for larger clusters power-law exponents between −1.6 and −1.1 are determined from the fits. An apparent lack of any correlation between the values of power-law exponents and polymer concentration, as well as a weak dependence of the cluster size distributions on fluence suggest that the bimodal power-law cluster size distribution may be a general characteristic of the ablation plume generated as a result of an explosive decomposition of a target region overheated above the limit of its thermodynamic stability.

Similar bimodal power-law cluster size distributions have been observed earlier in MD simulations of laser ablation of one-component molecular targets.[47] Moreover, recent analysis of high-resolution SEM images of thin polymer films deposited in MAPLE at three different laser fluences

Downloaded 11 Oct 2007 to 128.143.68.241. Redistribution subject to AIP license or copyright, see http://jap.aip.org/jap/copyright.jsp

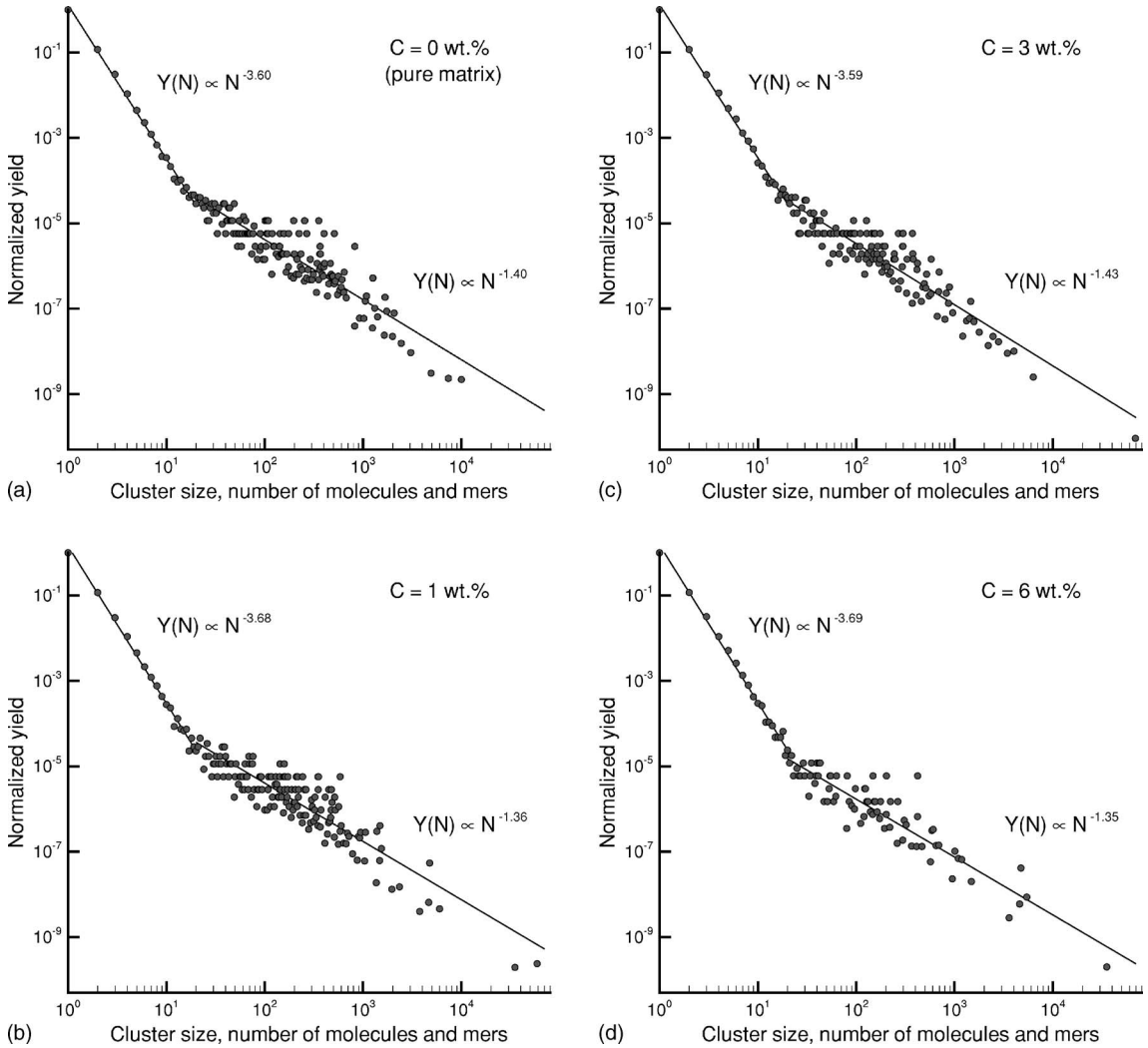

FIG. 10. Cluster size distributions in the ablation plume at 1 ns after the beginning of the laser pulse in simulations performed at a fluence of 8 mJ/cm^2 for pure matrix (a) and MAPLE targets with polymer concentrations of 1 (b), 3 (c), and 6 wt % (d). The yields of clusters are normalized to the number of individual matrix molecules shown in Fig. 5. Bimodal power-law distributions $Y(N) \propto N^{-t}$ are observed in all simulations, where N is the number of matrix molecules and polymer units (mers) in clusters.

reveals that the mass distributions of the distinct polymer surface features can be well described by a power law with

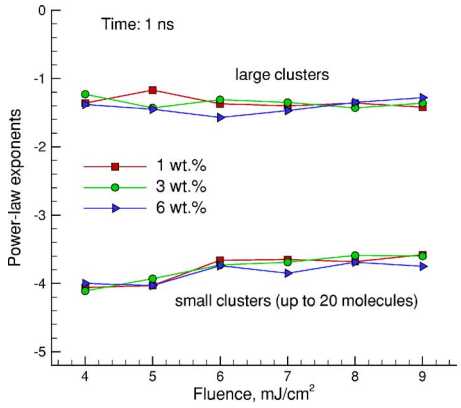

FIG. 11. (Color online) Fluence dependence of the exponents in the bimodal power-law fits of the cluster size distributions, such as the ones shown in Fig. 10. The exponents for small (up to 20 molecules) and large (more than 20 molecules) clusters are shown for 1 ns after the beginning of the laser pulse in simulations performed for MAPLE targets with polymer concentrations of 1 wt % (red squares), 3 wt % (green circles), and 6 wt % (blue triangles).

exponent of −1.6.[30,87] The results of the simulations presented in this paper suggest that the polymer molecules in MAPLE are ejected within large matrix clusters that have a weak cluster size dependence on the polymer concentration. Evaporation of the volatile matrix in-flight and after the deposition to the substrate is likely to be responsible for the formation of the surface polymer features observed in the SEM images of MAPLE deposited films. Therefore, the mass of the large matrix-polymer clusters and the mass of the polymer features generated by evaporation of matrix from the deposited clusters can be expected to have similar distributions. Indeed, the experimental power-law exponent of −1.6 is close to the ones predicted in the simulations for the high-mass parts of the cluster size distributions, from −1.6 to −1.1. An additional moderate decrease of the power-law exponent (increase of the absolute value) due to in-flight breakup processes at longer times can be expected in the simulated distributions, as suggested by recent MD simulations of long-term (up to 1 μs) evolution of clusters ejected in sputtering of gold targets.[88] This decrease would bring the range of the power-law exponents predicted in simulations

Downloaded 11 Oct 2007 to 128.143.68.241. Redistribution subject to AIP license or copyright, see http://jap.aip.org/jap/copyright.jsp

for the high-mass parts of the cluster size distributions even closer to the ones measured in the MAPLE experiments. Note that quantitative comparison of the actual sizes of molecular clusters ejected in MAPLE experiments and simulations is not possible. Much larger molecular clusters, comparable to the laser penetration depth, can be expected to be generated in MAPLE experiments (laser penetration depth is ~4.0 μm in experiments[30,87] and ~50 nm in simulations). Molecular-level simulations of such clusters are far beyond the current computational capabilities. Nevertheless, the fact that the simulations and experiments are performed in the same physical regime of thermal confinement (see Sec. II), as well as a good agreement between the cluster size distributions observed in the simulations and experiments, support the notion that the same ejection mechanisms are responsible for the generation of clusters in MAPLE simulations and experiments.

Interestingly, the observation of power-law cluster size distributions with different exponents for small and large clusters correlates with similar results obtained in sputtering experiments. While small exponents in the range from −9 to −3 typically result from power-law fits to the sputtering yields of small clusters measured in mass spectrometry methods,[89–91] larger exponents of around −2 are reported based on transmission electron microscopy (TEM) analysis of significantly larger clusters (more than 500 atoms) deposited on a TEM transparent collector grid.[92] Similarly, recent mass spectrometry analysis of the sputtering yield from an indium target bombarded with 15 keV Xe^+ ions reveals that a power-law distribution with smaller exponent of −3.9 is suitable for the description of the abundance of small clusters composed of less than 20 atoms, whereas a larger exponent of −2.1 results from the power-law fit for larger clusters.[93]

The close quantitative match between the cluster size distributions observed in sputtering and laser ablation simulations points to a possible similarity between the processes responsible for the material ejection in ion beam sputtering and laser ablation.[94–96] In particular, although the complex character of the ablation and sputtering processes makes it difficult to establish direct links to the existing theoretical models that predict power-law cluster size distributions,[97–100] the existence of the two, low- and high-mass, regions in the cluster size distributions may point to the different origins of the small and large clusters. Connecting to the processes leading to the ablation plume formation discussed in Sec. III, the majority of monomers and small clusters are released in the explosive decomposition of the overheated material into the liquid and vapor, whereas the larger clusters appear as a result of decomposition and coarsening of the transient structure of interconnected liquid regions.[47] Similarly, the ejection of small clusters in sputtering experiments has been attributed to the fast collisional processes immediately following the ion impact, whereas generation of large clusters is related to collective atomic motions occurring at longer time scales.[93]

V. TARGET MODIFICATION BY A LASER PULSE: IMPLICATIONS FOR MULTIPULSE IRRADIATION REGIME

Experimentally, MAPLE film depositions are always performed in a multipulse laser irradiation regime and significant structural, morphological, and compositional changes may accumulate in the surface region of a target irradiated by multiple laser pulses. Even though the direct MD simulation of the effect of repetitive multipulse laser irradiation is not feasible, analysis of the state of the target after irradiation by a single laser pulse can provide insights into the character of changes in the ablation process that may be associated with multipulse irradiation.

Snapshots of the MAPLE target surfaces taken at the ends of the simulations, Fig. 12, reveal general characteristics of the new surface regions left behind by the ablation process. The initial polymer concentration appears to be an important factor defining the dynamics of the material ejection and the final surface morphology. In the simulations performed for targets with 1 wt % polymer loading, Fig. 12(a), the new surfaces tend to be smooth. The relatively small bumps, observed for simulations performed at 5 and 7 mJ/cm^2, are likely to spread along the surface and disappear with time. On the contrary, the surfaces generated by laser ablation of MAPLE targets with 3 and 6 wt % polymer concentrations exhibit much higher degree of roughness, with elongated filaments observed in many of the simulations. The filaments are generated in the course of the decomposition of the foamy transient liquid-vapor structure emerged from the explosive decomposition of the overheated surface region of the target (see Sec. III). The presence of polymer chains in MAPLE targets stabilizes the liquid structures, increases viscosity of the matrix-polymer solution, and slows down the morphological relaxation of the surface. Fast evaporation of the volatile matrix molecules leads to both cooling of the surface structures and increase in the polymer concentration in the surface region of the target. Large surface-to-volume ratio of the filament structures facilitates the evaporative cooling and eventual freezing/solidification of the surface morphologies. One can expect, therefore, that the final resolidified surfaces would have complex morphologies that would include bumps, voids, complex meshlike structures, as well as a prominent presence of collapsed elongated filaments. The formation of elongated filaments can be related to experimental observations of "nanofibers" produced by laser ablation on surfaces of polymer and biopolymer targets.[62–65] While the initial state of the targets used in these experiments is different from polymer solution used in MAPLE, pulsed laser irradiation of a polymer target generates a viscous fluid composed of overheated volatile products of photothermal and photochemical polymer decomposition reactions mixed with polymer molecules and fragments, bringing the state of the material in the surface region of the irradiated target closer to the one characteristic for MAPLE experiments.

In addition to the formation of rough target surface morphology, simulations predict that the composition of the surface region of the target can be significantly altered by the ablation process. The time evolution of the average tempera-

Downloaded 11 Oct 2007 to 128.143.68.241. Redistribution subject to AIP license or copyright, see http://jap.aip.org/jap/copyright.jsp

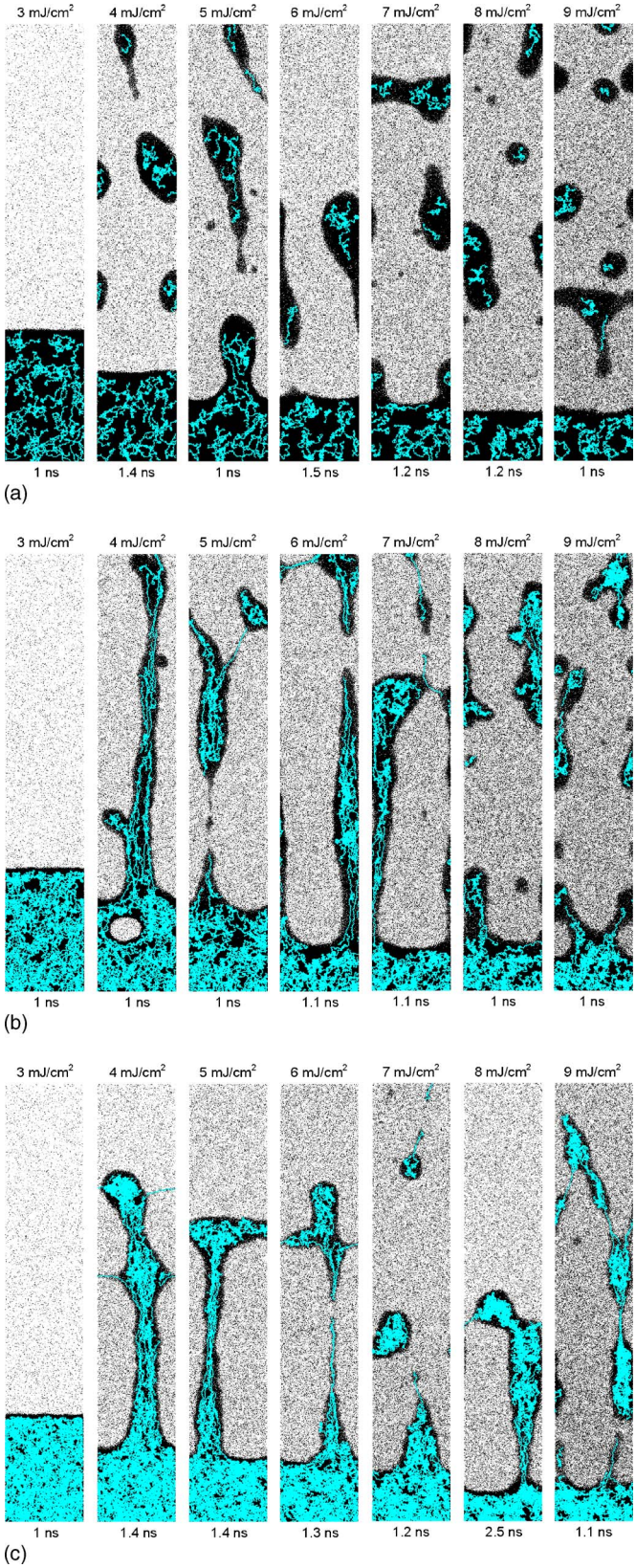

FIG. 12. (Color online) Snapshots of the target surface region taken at the end of the simulations performed for MAPLE targets with polymer concentrations of 1 (a), 3 (b), and 6 wt % (c). Laser fluences are shown above the snapshots and the times the snapshots are taken are shown below the snapshots. The polymer chains are shown in blue and are superimposed on top of the image of matrix molecules shown in the background.

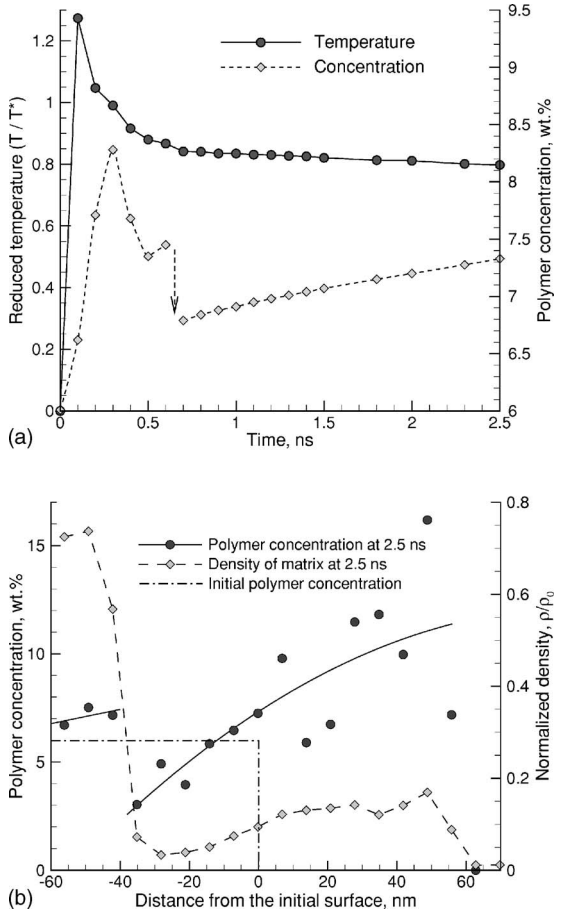

FIG. 13. Evolution of the average temperature and the polymer concentration in the surface region of a MAPLE target with initial polymer concentration of 6 wt % irradiated by a 50 ps laser pulse at a laser fluence of 8 mJ/cm^2 (a), and the distributions of the polymer concentration and the density of the molecular material at the end of the simulation (b). The values of temperature and concentration in (a) are averaged over the remaining part of the original 60 nm deep surface region represented in the simulation. The temperature values in (a) are normalized to the threshold temperature for the phase explosion, T^*. The density of the molecular material in (b) is normalized to the density in the original target, ρ_0. The initial polymer concentration profile is shown schematically by a dash-dotted line, whereas the solid lines are just guides to the eye showing trends in the variation of the polymer concentration in (b). The arrow in (a) corresponds to the separation of a large cluster, shown in the left inset in Fig. 7(a), from the target at 650 ps.

ture and polymer concentration in a MAPLE target with an initial concentration of 6 wt % irradiated at a laser fluence of 8 mJ/cm^2 is shown in Fig. 13(a). The values of temperature and concentration are averaged over the remaining part of the original 60 nm deep surface region represented in the MD simulation. This region is gradually shrinking during the ablation process due to the emission of molecules and clusters. The initial sharp increase of the polymer concentration during the first 300 ps corresponds to the active evaporation of matrix molecules from the surface. The evaporation continues past 300 ps but the average concentration of the target drops due to the disintegration of the transient foamy matrix-polymer structure and separation of multiple polymer-rich clusters, see Fig. 2(d) and a frame for 8 mJ/cm^2 in Fig. 3(c). The emission of clusters ceases by ~500 ps and evaporation from an extended liquid structure connected to the target [see snapshot at 600 ps in Fig. 2(d)] contributes to the additional increase of the average polymer concentration of the target. A large part of this liquid polymer-rich structure separates at

Downloaded 11 Oct 2007 to 128.143.68.241. Redistribution subject to AIP license or copyright, see http://jap.aip.org/jap/copyright.jsp

~650 ps [see snapshot at 800 ps in Fig. 2(d) and an inset in Fig. 7(a)], leading to the drop of the average polymer concentration shown by the arrow in Fig. 13(a). Further increase of the polymer concentration in the surface region of the target corresponds to the continued evaporation of matrix molecules. The gradual decrease of the rate of the polymer concentration increase (slope of the concentration—time dependence) after 700 ps corresponds to a slow evaporative cooling of the surface, whereas a discontinuous change of the rate from 600 to 700 ps corresponds to the drop in the surface area due to the separation of the elongated liquid droplet at ~650 ps.

Note that the temperature of the target at the end of the simulation, 2.5 ns, is $0.8T^*$, significantly higher than the temperature of the large clusters ejected in this simulation, ranging from 0.70 to $0.73T^*$, Fig. 7. This observation seems counterintuitive at the first sight, as the clusters are ejected from the upper regions of the target where the energy density deposited by the laser pulse is higher. The lower temperature of the clusters, however, can be explained by the fast initial cooling provided by a vigorous explosive phase separation occurring in the upper part of the target, as well as by a more active evaporative cooling at later times due to the large surface-to-volume ratio in the clusters.

The distributions of the polymer concentration and the density of the molecular material at the end of the simulation are shown in Fig. 13(b). The density distribution reflects the visual picture of the surface morphology shown in a frame for 8 mJ/cm^2 in Fig. 12(c). The density below −40 nm corresponds to almost 80% of the initial density of the frozen target and we can define this level as a ground level of the new surface. The polymer concentration in the new surface region of the target (below −40 nm) is higher than the original 6 wt % concentration by ~1 wt %. The average polymer concentration in the elongated liquid structure connected to the target is significantly higher than the original one and increases up to more than 10 wt % further away from the new target surface. The only region where the polymer concentration is below the original 6 wt % is a thin molecular bridge (from −40 to −15 nm) connecting the extended liquid droplet with the bulk of the target. The average velocity of the liquid structure in the direction normal to the surface is still positive (directed away from the target) and has a value of 20 m/s. It is possible that the liquid structure would separate from the target at a later time. Similarly, positive average velocity of 1 m/s is calculated for the liquid structure sticking out of the new surface in a simulation with $C=6$ wt % and $F=5$ mJ/cm^2, Fig. 12(c), and average velocity of 53 m/s is calculated for the liquid structure in a simulation with $C=3$ wt % and $F=7$ mJ/cm^2, Fig. 12(b). Regardless of the outcomes of these particular simulations, all of the following scenarios of the fate of the large elongated polymer-rich liquid droplets are possible: freezing and collapse on the target surface contributing to the formation of the complex surface morphology; separation and slow flight away from the target with possible deposition to the substrate contributing to the roughness of the deposited polymer films; and separation and redeposition to the target within or outside the laser spot.

Although the increase of the polymer concentration in the surface region of the irradiated target is not dramatic and is limited to one to several wt %, the molecular ejection is clearly nonstoichiometric and becomes more nonstoichiometric with time (average polymer concentration in the plume in the simulation illustrated in Fig. 13 is 4.98 wt % at 1.5 ns, 4.89 wt % at 2 ns, and 4.81 wt % at 2.5 ns). One can expect that the effect of the increasing polymer concentration in the target may accumulate in the course of repetitive multipulse irradiation, especially at low laser fluences, close to the ablation threshold, and for targets with low initial polymer loading. As the concentration of polymer molecules in the surface region of the target increases, a polymer density gradient may hamper the evaporation of the volatile matrix vapor generated in a subsurface region, leading to the formation of voids, bubbles, and overall swelling and foaming of the target, as observed in a recent MAPLE experiment[69] and commonly reported for laser ablation of polymers and biological tissues.[65–68] This scenario has a common origin with the formation of a polymer density gradient acting as a barrier for solvent evaporation from a solvent-polymer system[101] investigated in recent MD simulations,[102] as well as with the generation of transient "molecular balloons" revealed in the simulations of the evolution of matrix-polymer droplets ejected in MAPLE.[32]

In addition to the direct effect on the mechanisms of molecular ejection, the compositional and morphological changes in the surface region can have implications on optical properties of the surface, thermodynamic properties of the laser-modified target material, and even heat transfer mechanisms in the heat-affected region of the target.[68]

VI. DISCUSSION OF THE IMPLICATIONS FOR MAPLE

The development of MAPLE technique has been driven by the desire to achieve deposition of ultrathin homogeneous organic films with precise thickness control and minimum modification of the chemical structure and functionality of the deposited molecules. Thus, two main objectives of MAPLE are as follow: (1) to avoid photochemical and photothermal molecular fragmentation (bond scission), characteristic for PLD, and (2) to achieve deposition of highly uniform thin films that cannot be produced by solvent-based coating methods. These objectives are thought to be met by achieving a soft matrix-assisted ejection and deposition of individual molecules with minimal thermal or photochemical fragmentation.

The simulations presented in this paper do support the notion of minimal chemical modification of polymer molecules in MAPLE film deposition, also confirmed in a recent MALDI mass spectrometry analysis of poly(3-hexylthiophene) (P3HT) films deposited by MAPLE.[27] Indeed, we do not detect any photothermal bond scission events in any of the simulations performed for polymer concentrations up to 6 wt % and laser fluences up to more than twice the ablation threshold. Although more violent phase explosion at higher fluences or stronger polymer entanglement at larger polymer concentrations may cause some bond-breaking reactions, the fraction of the broken bonds would

Downloaded 11 Oct 2007 to 128.143.68.241. Redistribution subject to AIP license or copyright, see http://jap.aip.org/jap/copyright.jsp

still be significantly smaller than in the ablation of polymer targets in PLD. In fact, the purely photothermal model for laser ablation of polymer targets stipulates a certain critical number of broken chemical bonds for the initiation of the ablation process, e.g., Refs. 103–105. In recent MD simulations of polymer ablation[106] it was found that in the thermal regime, without direct photofragmentation reactions, the critical number of broken chemical bonds is about 10% even for small PMMA molecules (19-mers). The critical fraction of the broken bonds is likely to be higher for polymers with higher molecular weight, as suggested by recent experimental investigations.[67,107] Thus, while the dissociation of chemical bonds appears to be unavoidable in PLD, MAPLE technique provides an attractive opportunity for deposition of polymer molecules without any significant chemical modification and reduction of the molecular weight.

Another premise of MAPLE, the fabrication of smooth films through molecule-by-molecule deposition, appears to be more challenging, if not impossible, to achieve. Our simulations show that polymer molecules are always ejected as parts of matrix-polymer clusters with a broad cluster size distribution. The ejection of molecular clusters and droplets is inherently connected to the basic mechanism of laser ablation—explosive decomposition of a surface region of the target overheated up to the limit of its thermodynamic stability. The simulations predict that the "phase explosion" proceeds through the formation of a foamy transient structure of interconnected liquid regions that subsequently decomposes into a mixture of liquid droplets and gas-phase matrix molecules. Smaller clusters tend to originate from the upper parts of the emerging ablation plume, whereas larger droplets are lagging behind and tend to have smaller ejection velocities, but all of these clusters/droplets are unavoidable products of the collective material ejection process (ablation).

The presence of polymer molecules in MAPLE targets stabilizes the transient liquid structures generated in the explosive disintegration of the overheated matrix, increases viscosity of the liquid, and facilitates the formation of intricate elongated structures that can either reach the substrate and contribute to the roughness of the deposited film or remain at the target, leading to the formation of complex surface morphology. Although the results of the simulations go against the original notion of the ejection and transport of individual polymer molecules in MAPLE,[1–3] they provide an explanation for the significant surface roughness often observed upon close examination of the deposited films, e.g., Refs. 11, 14, 18, 24, 25, and 27–32. Moreover, the unusual elongated shapes of the deposited surface features[18,30,87] can be related to the formation and ejection of long filaments observed in the simulations. The ejection of the filaments becomes more pronounced with increasing polymer concentration in the target.

The wrinkled "deflated balloon" surface features, observed in recent MAPLE experiments,[18,30] can also be explained based on the ejection of large matrix-polymer droplets predicted in the simulations.[32] It has been demonstrated in a series of targeted MD simulations that an internal release of the matrix vapor in a large matrix-polymer droplet is capable of pushing the polymer molecules to the outskirts of the droplet, thus forming a transient molecular balloon expanding under the action of the internal vapor pressure. Active evaporation of matrix molecules from the surface of the droplet contributes to the formation of a polymer-rich surface layer, hampering the escape of the remaining matrix molecules. Following the deposition of the molecular balloon on a room-temperature substrate, the volatile matrix material enclosed by a polymer-rich layer expands and makes escape passes through the polymer layer, leaving behind characteristic wrinkled polymer structures. This scenario is schematically illustrated in Fig. 14 and discussed in more detail in Ref. 32.

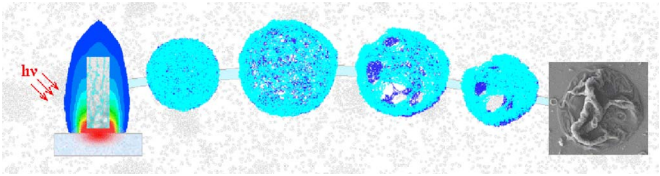

FIG. 14. (Color online) Schematic representation of the scenario for the formation of the experimentally observed "deflated balloon" surface features suggested based on the results of the simulations discussed in Ref. 32.

The following important practical question follows from the above discussion of the simulation results. Is it possible to avoid or minimize the deposition of molecular clusters in MAPLE and achieve a molecule-by-molecule deposition of ultrathin polymer films without any significant roughness by selecting an appropriate set of MAPLE parameters? Below we briefly discuss some of the possible directions aimed at eliminating or minimizing the cluster ejection in MAPLE.

(I) An increase in the laser pulse duration may result in the rates of laser energy deposition commensurate with the surface evaporation regime. While evaporation from the surface would not involve cluster ejection, the evaporating matrix molecules are unlikely to entrain any polymer molecules. Indeed, in MALDI experiments measuring both directly ejected ions and postionized neutral molecules, the neutral matrix molecules are observed at lower laser fluences as compared to the analyte molecules (and ions).[77] Computational investigations of MALDI mechanisms[40] provide explanation of these observations by suggesting that the ejection of large analyte molecules can only take place above the threshold for collective ejection of matrix (ablation), whereas evaporation of matrix molecules starts at significantly lower fluences. Another analogy illustrating the inability of evaporation to provide conditions for molecular entrainment can be drawn to buffer-layer-assisted methods for deposition of metal clusters and laser patterning.[108–110] In these methods, a buffer layer made of frozen inert gas atoms or volatile molecules is exposed to atoms evaporated from a hot source, leading to condensation of small polyatomic clusters of the source material. In the following slow thermal annealing, the buffer layer atoms evaporate around the deposited clusters, leading to the soft landing of the clusters to the substrate. The removal of the clus-

Downloaded 11 Oct 2007 to 128.143.68.241. Redistribution subject to AIP license or copyright, see http://jap.aip.org/jap/copyright.jsp

ters requires much larger heating rates that can be achieved by short pulse laser irradiation leading to the fast collective ejection (ablation) of the buffer layer.[109,110] Thus, one can conclude that evaporation, the process originally thought to be responsible for the molecular transfer in MAPLE and ingrained in the name of the technique, matrix-assisted pulsed laser *evaporation*, cannot be used for deposition of thin films composed of intact polymer molecules.

(II) A decrease of the polymer concentration in a MAPLE target would result in smaller amounts of polymer material in the ejected clusters, thus reducing the size of the polymer features generated within the growing film by evaporation of the volatile matrix from the deposited matrix-polymer clusters. The formation of the extended filaments is also minimized at low polymer concentrations [e.g., compare the shapes of the large droplets in Fig. 12(a) with the ones in Figs. 12(b) and 12(c)]. The problem with using MAPLE targets with low polymer concentrations is the decrease of the efficiency of the technique for the polymer film fabrication. Moreover, the polymer concentration in the surface region of the target can go up in a multipulse irradiation regime, as suggested by the analysis presented in Sec. V.

(III) Assuming that the ejection of matrix-polymer clusters (and associated nonuniform deposition of the polymer material) is unavoidable in MAPLE, the roughness of the growing films can be, at least partially, controlled by changing the temperature of the substrate. Indeed, the initial studies of the effect of the substrate temperature[25,27,69] on the morphology of films deposited in MAPLE indicate that individual surface features become less distinct as the substrate temperature approaches or exceeds the polymer glass transition temperature, and disappear/merge at temperatures close to the polymer melting temperature.[25] The prominent presence of matrix molecules in the clusters/droplets reaching the substrate, predicted in the simulations, should be taken into account in interpretation of the temperature effect on the roughness of the deposited film. In particular, the glass transition temperature of the deposited polymeric material can be significantly reduced by the presence of residual matrix molecules, explaining the observation of changes in the shapes of the deposited surface features at temperatures well below the glass transition temperature of the deposited polymer.[69] An observation of a significant increase in roughness of MAPLE-deposited P3HT films observed as substrate temperature is elevated from −30 °C (below the melting temperature of orthoxylene used as matrix, −25 °C) to the room temperature[27] may also be related to the redistribution and evaporation of the matrix content of the deposited film at the higher temperature. Thus, while the underlying processes responsible for the temperature dependence of the roughness of MAPLE-deposited films are not completely understood and may be affected by the thermodynamic and thermochemical properties of matrix and polymer molecules, the control of the substrate temperature and postdeposition thermal treatment are providing additional avenues for improving the uniformity of the deposited films.

ACKNOWLEDGMENTS

The authors would like to thank Aaron T. Sellinger and James M. Fitz-Gerald of the University of Virginia and Yasuyuki Tsuboi of the Hokkaido University for useful suggestions and discussions. Financial support of this work is provided by the National Science Foundation through Grants No. DMII-0422632 and NIRT-0403876.

[1] A. Piqué, R. A. McGill, D. B. Chrisey, J. Callahan, and T. E. Mlsna, *Advances in Laser Ablation of Materials*, edited by R. K. Singh, D. H. Lowndes, D. B. Chrisey, J. Narayan, T. Kawai, and E. Fogarassy, MRS Symposia Proceedings No. 526 (MRS, Warrendale, PA, 1998), p. 375.
[2] A. Piqué, R. A. McGill, D. B. Chrisey, D. Leonhardt, T. E. Mslna, B. J. Spargo, J. H. Callahan, R. W. Vachet, R. Chung, and M. A. Bucaro, Thin Solid Films **355/356**, 536 (1999).
[3] D. B. Chrisey, A. Piqué, R. A. McGill, J. S. Horwitz, B. R. Ringeisen, D. M. Bubb, and P. K. Wu, Chem. Rev. (Washington, D.C.) **103**, 553 (2003).
[4] P. K. Wu, B. R. Ringeisen, D. B. Krizman, C. G. Frondoza, M. Brooks, D. M. Bubb, R. C. Y. Auyeung, A. Piqué, B. Spargo, R. A. McGill, and D. B. Chrisey, Rev. Sci. Instrum. **74**, 2546 (2003).
[5] M. Jelinek, T. Kocourek, J. Remsa, R. Cristescu, I. N. Mihailescu, and D. B. Chrisey, Laser Phys. **17**, 66 (2007).
[6] T. M. Patz, A. Doraiswamy, R. J. Narayan, N. Menegazzo, C. Kranz, B. Mizaikoff, Y. Zhong, R. Bellamkonda, J. D. Bumgardner, S. H. Elder, X. F. Walboomers, R. Modi, and D. B. Chrisey, Mater. Sci. Eng., C **27**, 514 (2007).
[7] A. Piqué, P. Wu, B. R. Ringeisen, D. M. Bubb, J. S. Melinger, R. A. McGill, and D. B. Chrisey, Appl. Surf. Sci. **186**, 408 (2002).
[8] A. Piqué, R. C. Y. Auyeung, J. L. Stepnowski, D. W. Weir, C. B. Arnold, R. A. McGill, and D. B. Chrisey, Surf. Coat. Technol. **163**, 293 (2003).
[9] J. M. Fitz-Gerald, G. Jennings, R. Johnson, and C. L. Fraser, Appl. Phys. A: Mater. Sci. Process. **80**, 1109 (2005).
[10] E. J. Houser, D. B. Chrisey, M. Bercu, N. D. Scarisoreanu, A. Purice, D. Colceag, C. Constantinescu, A. Moldovan, and M. Dinescu, Appl. Surf. Sci. **252**, 4871 (2006).
[11] R. Fryček, M. Jelínek, T. Kocourek, P. Fitl, M. Vrňata, V. Myslík, and M. Vrbová, Thin Solid Films **495**, 308 (2006).
[12] B. R. Ringeisen, J. Callahan, P. K. Wu, A. Piqué, B. Spargo, R. A. McGill, M. Bucaro, H. Kim, D. M. Bubb, and D. B. Chrisey, Langmuir **17**, 3472 (2001).
[13] L. Stamatin, R. Cristescu, G. Socol, A. Moldovan, D. Mihaiescu, I. Stamatin, I. N. Mihailescu, and D. B. Chrisey, Appl. Surf. Sci. **248**, 422 (2005).
[14] R. Cristescu, D. Mihaiescu, G. Socol, I. Stamatin, I. N. Mihailescu, and D. B. Chrisey, Appl. Phys. A: Mater. Sci. Process. **79**, 1023 (2004).
[15] A. Purice, J. Schou, P. Kingshott, N. Pryds, and M. Dinescu, Appl. Surf. Sci. **253**, 6451 (2007).
[16] A. Purice, J. Schou, P. Kingshott, and M. Dinescu, Chem. Phys. Lett. **435**, 350 (2007).
[17] P. K. Wu, J. Fitz-Gerald, A. Piqué, D. B. Chrisey, and R. A. McGill, *Laser-Solid interactions for Materials Processing*, edited by D. Kumar, D. P. Norton, C. B. Lee, K. Ebihara, and X. X. Xi, MRS Symposia Proceedings No. 617 (MRS, Warrendale, PA, 2000), p. J2.3.1.
[18] A. T. Sellinger, E. M. Leveugle, K. Gogick, L. V. Zhigilei, and J. M. Fitz-Gerald, J. Vac. Sci. Technol. A **24**, 1618 (2006).
[19] A. P. Caricato, M. G. Manera, M. Martino, R. Rella, F. Romano, J. Spadavecchia, T. Tunno, and D. Valerini, Appl. Surf. Sci. **253**, 6471 (2007).
[20] B. Toftmann, M. R. Papantonakis, R. C. Y. Auyeung, W. Kim, S. M. O'Malley, D. M. Bubb, J. S. Horwitz, J. Schou, P. M. Johansen, and R. F. Haglund, Thin Solid Films **453–454**, 177 (2004).
[21] D. M. Bubb, S. M. O'Malley, C. Antonacci, D. Simonson, and R. A. McGill, J. Appl. Phys. **95**, 2175 (2004).
[22] D. M. Bubb, A. O. Sezer, J. Gripenburg, B. Collins, and E. Brookes, Appl. Surf. Sci. **253**, 6465 (2007).

Downloaded 11 Oct 2007 to 128.143.68.241. Redistribution subject to AIP license or copyright, see http://jap.aip.org/jap/copyright.jsp

[23]D. M. Bubb, P. K. Wu, J. S. Horwitz, J. H. Callahan, M. Galicia, A. Vertes, R. A. McGill, E. J. Houser, B. R. Ringeisen, and D. B. Chrisey, J. Appl. Phys. **91**, 2055 (2002).
[24]B. Toftmann, K. Rodrigo, J. Schou, and R. Pedrys, Appl. Surf. Sci. **247**, 211 (2005).
[25]K. Rodrigo, P. Czuba, B. Toftmann, J. Schou, and R. Pedrys, Appl. Surf. Sci. **252**, 4824 (2006).
[26]A. Purice, J. Schou, and M. Dinescu, Chem. Phys. Lett. **427**, 251 (2006).
[27]A. Gutiérrez-Llorente, G. Horowitz, R. Pérez-Casero, J. Perrière, J. L. Fave, A. Yassar, and C. Sant, Org. Electron. **5**, 29 (2004).
[28]A. Gutierrez-Llorente, R. Perez-Casero, B. Pajot, J. Roussel, R. M. Defourneau, D. Defourneau, J. L. Fave, E. Millon, and J. Perriere, Appl. Phys. A: Mater. Sci. Process. **77**, 785 (2003).
[29]A. L. Mercado, C. E. Allmond, J. G. Hoekstra, and J. M. Fitz-Gerald, Appl. Phys. A: Mater. Sci. Process. **81**, 591 (2005).
[30]A. T. Sellinger, E. Leveugle, K. Gogick, G. Peman, L. V. Zhigilei, and J. M. Fitz-Gerald, J. Phys.: Conf. Ser. **59**, 314 (2007).
[31]E. Leveugle, L. V. Zhigilei, A. Sellinger, and J. M. Fitz-Gerald, J. Phys.: Conf. Ser. **59**, 126 (2007).
[32]E. Leveugle, A. Sellinger, J. M. Fitz-Gerald, and L. V. Zhigilei, Phys. Rev. Lett. **98**, 216101 (2007).
[33]A. Bencsura, V. Navale, M. Sadeghi, and A. Vertes, Rapid Commun. Mass Spectrom. **11**, 679 (1997).
[34]X. Wu, M. Sadeghi, and A. Vertes, J. Phys. Chem. B **102**, 4770 (1998).
[35]Y. Dou, N. Winograd, B. J. Garrison, and L. V. Zhigilei, J. Phys. Chem. B **107**, 2362 (2003).
[36]M. Sadeghi, X. Wu, and A. Vertes, J. Phys. Chem. B **105**, 2578 (2001).
[37]L. V. Zhigilei and B. J. Garrison, Rapid Commun. Mass Spectrom. **12**, 1273 (1998).
[38]T. E. Itina, L. V. Zhigilei, and B. J. Garrison, Nucl. Instrum. Methods Phys. Res. B **180**, 238 (2001).
[39]T. E. Itina, L. V. Zhigilei, and B. J. Garrison, J. Phys. Chem. B **106**, 303 (2002).
[40]L. V. Zhigilei, Y. G. Yingling, T. E. Itina, T. A. Schoolcraft, and B. J. Garrison, Int. J. Mass Spectrom. **226**, 85 (2003).
[41]M. Karas, D. Bachmann, U. Bahr, and F. Hillenkamp, Int. J. Mass Spectrom. Ion Process. **78**, 53 (1987).
[42]F. Hillenkamp, M. Karas, R. C. Beavis, and B. T. Chait, Anal. Chem. **63**, 1193A (1991).
[43]K. Dreisewerd, Chem. Rev. (Washington, D.C.) **103**, 395 (2003).
[44]L. V. Zhigilei, P. B. S. Kodali, and B. J. Garrison, J. Phys. Chem. B **101**, 2028 (1997).
[45]*Computer Simulation of Polymers*, edited by E. A. Colbourn (Longman Scientific and Technical, Harlow, 1994).
[46]L. V. Zhigilei and B. J. Garrison, J. Appl. Phys. **88**, 1281 (2000).
[47]L. V. Zhigilei, Appl. Phys. A: Mater. Sci. Process. **76**, 339 (2003).
[48]L. V. Zhigilei, E. Leveugle, B. J. Garrison, Y. G. Yingling, and M. I. Zeifman, Chem. Rev. (Washington, D.C.) **103**, 321 (2003).
[49]A. I. Kitaigorodsky, *Molecular Crystals and Molecules* (Academic, New York, 1993).
[50]*CRC Handbook of Chemistry and Physics*, 87th ed., edited by D. R. Lide (CRC, Boca Raton, FL, 1996).
[51]J. D. Moore, S. T. Cui, H. D. Cochran, and P. T. Cummings, J. Non-Newtonian Fluid Mech. **93**, 83 (2000).
[52]L. V. Zhigilei and B. J. Garrison, *Multiscale Modelling of Materials*, edited by V. V. Bulatov, T. Diaz de la Rubia, R. Phillips, E. Kaxiras, and N. Ghoniem, MRS Symposia Proceeding No. 538 (MRS, Warrendale, PA, 1999), p. 491.
[53]A. Vogel and V. Venugopalan, Chem. Rev. (Washington, D.C.) **103**, 577 (2003).
[54]G. Paltauf and P. E. Dyer, Chem. Rev. (Washington, D.C.) **103**, 487 (2003).
[55]*Kaye and Laby Online Tables of Physical and Chemical Constants* (National Physical Laboratory, Teddington, Middlesex, 2007); ⟨http://www.kayelaby.npl.co.uk/⟩.
[56]Y. Tsuboi, K. Hatanaka, H. Fukumura, and H. Masuhara, J. Phys. Chem. **98**, 11237 (1994).
[57]A. Koubenakis, T. Elimioti, and S. Georgiou, Appl. Phys. A: Mater. Sci. Process. **69**, S637 (1999).
[58]A. Miotello and R. Kelly, Appl. Phys. A: Mater. Sci. Process. **69**, S67 (1999).
[59]N. M. Bulgakova and I. M. Bourakov, Appl. Surf. Sci. **197**, 41 (2002).
[60]B. J. Garrison, T. E. Itina, and L. V. Zhigilei, Phys. Rev. E **68**, 041501 (2003).
[61]J. Blazevska-Gilev, J. Kupčík, J. Šubrt, Z. Bastl, V. Vorlíček, A. Galíková, D. Spaseska, and J. Pola, Polym. Degrad. Stab. **91**, 213 (2006).
[62]F. Weisbuch, V. N. Tokarev, S. Lazare, C. Belin, and J. L. Bruneel, Appl. Phys. A: Mater. Sci. Process. **75**, 677 (2002).
[63]F. Weisbuch, V. N. Tokarev, S. Lazare, C. Belin, and J. L. Bruneel, Thin Solid Films **453**, 394 (2004).
[64]V. N. Tokarev, Laser Phys. **16**, 1291 (2006).
[65]R. Srinivasan, K. G. Casey, B. Braren, and M. Yeh, J. Appl. Phys. **67**, 1604 (1990).
[66]S. Lazare, V. Tokarev, A. Sionkowska, and M. Wiśniewski, Appl. Phys. A: Mater. Sci. Process. **81**, 465 (2005).
[67]E. Rebollar, G. Bounos, M. Oujja, S. Georgiou, and M. Castillejo, J. Phys. Chem. B **110**, 16452 (2006).
[68]A. Malyshev and N. Bityurin, Appl. Phys. A: Mater. Sci. Process. **79**, 1175 (2004).
[69]A. Sellinger and J. M. Fitz-Gerald, (private communication).
[70]L. V. Zhigilei and B. J. Garrison, Appl. Phys. Lett. **74**, 1341 (1999).
[71]L. V. Zhigilei and B. J. Garrison, Appl. Phys. A: Mater. Sci. Process. **69**, S75 (1999).
[72]A. Koubenakis, J. Labrakis, and S. Georgiou, Chem. Phys. Lett. **346**, 54 (2001).
[73]J. H. Brannon, J. R. Lankard, A. I. Baise, F. Burns, and J. Kaufman, J. Appl. Phys. **58**, 2036 (1985).
[74]R. Srinivasan and B. Braren, Chem. Rev. (Washington, D.C.) **89**, 1303 (1989).
[75]C. Mihesan, M. Ziskind, B. Chazallon, E. Therssen, P. Desgroux, and C. Focsa, Surf. Sci. **593**, 221 (2005).
[76]C. Mihesan, M. Ziskind, B. Chazallon, E. Therssen, P. Desgroux, S. Gurlui, and C. Focsa, Appl. Surf. Sci. **253**, 1090 (2006).
[77]K. Dreisewerd, M. Schürenberg, M. Karas, and F. Hillenkamp, Int. J. Mass Spectrom. Ion Process. **141**, 127 (1995).
[78]M. Schürenberg, K. Dreisewerd, S. Kamanabrou, and F. Hillenkamp, Int. J. Mass Spectrom. Ion Process. **172**, 89 (1998).
[79]C. Focsa, C. Mihesan, M. Ziskind, B. Chazallon, E. Therssen, P. Desgroux, and J. L. Destombes, J. Phys.: Condens. Matter **18**, S1357 (2006).
[80]C. Mihesan, M. Ziskind, E. Therssen, P. Desgroux, and C. Focsa, Chem. Phys. Lett. **423**, 407 (2006).
[81]J. W. Elam and D. H. Levy, J. Phys. Chem. B **102**, 8113 (1998).
[82]W. Zhang and B. T. Chait, Int. J. Mass Spectrom. Ion Process. **160**, 259 (1997).
[83]T. Huth-Fehre and C. H. Becker, Rapid Commun. Mass Spectrom. **5**, 378 (1991).
[84]Y. Pan and R. J. Cotter, Org. Mass Spectrom. **27**, 3 (1992).
[85]A. A. Puretzky, D. B. Geohegan, G. B. Hurst, M. V. Buchanan, and B. S. Luk'yanchuk, Phys. Rev. Lett. **83**, 444 (1999).
[86]S. Berkenkamp, C. Menzel, F. Hillenkamp, and K. Dreisewerd, J. Am. Soc. Mass Spectrom. **13**, 209 (2002).
[87]E. Leveugle, L. V. Zhigilei, A. Sellinger, and J. M. Fitz-Gerald, Appl. Surf. Sci. **253**, 6456 (2007).
[88]K. O. E. Henriksson, K. Nordlund, and J. Keinonen, Phys. Rev. B **71**, 014117 (2005).
[89]C. Staudt, R. Heinrich, and A. Wucher, Nucl. Instrum. Methods Phys. Res. B **164**, 677 (2000).
[90]S. R. Coon, W. F. Calaway, M. J. Pellin, and J. M. White, Surf. Sci. **298**, 161 (1993).
[91]T. J. Colla, H. M. Urbassek, A. Wucher, C. Staudt, R. Heinrich, B. J. Garrison, C. Dandachi, and G. Betz, Nucl. Instrum. Methods Phys. Res. B **143**, 284 (1998).
[92]L. E. Rehn, R. C. Birtcher, S. E. Donnelly, P. M. Baldo, and L. Funk, Phys. Rev. Lett. **87**, 207601 (2001).
[93]C. Staudt and A. Wucher, Phys. Rev. B **66**, 075419 (2002).
[94]R. Kelly and A. Miotello, Nucl. Instrum. Methods Phys. Res. B **141**, 49 (1998).
[95]R. Kelly and A. Miotello, Mater. Sci. Eng., A **253**, 178 (1998).
[96]R. Kelly and A. Miotello, Phys. Rev. E **60**, 2616 (1999).
[97]H. M. Urbassek, Nucl. Instrum. Methods Phys. Res. B **31**, 541 (1988).
[98]A. Bershadskii, Eur. Phys. J. B **14**, 323 (2000).
[99]I. S. Bitensky and E. S. Parilis, Nucl. Instrum. Methods Phys. Res. B **21**, 26 (1987).
[100]L. E. Rehn, R. C. Birtcher, P. M. Baldo, A. W. McCormick, and L. Funk, Nucl. Instrum. Methods Phys. Res. B **212**, 326 (2003).

Downloaded 11 Oct 2007 to 128.143.68.241. Redistribution subject to AIP license or copyright, see http://jap.aip.org/jap/copyright.jsp

[101] T. Okuzono, K. Ozawa, and M. Doi, Phys. Rev. Lett. **97**, 136103 (2006).
[102] M. Tsige and G. S. Grest, Macromolecules **37**, 4333 (2004).
[103] N. Bityurin, B. S. Luk'yanchuk, M. H. Hong, and T. C. Chong, Chem. Rev. (Washington, D.C.) **103**, 519 (2003).
[104] N. Bityurin and A. Malyshev, J. Appl. Phys. **92**, 605 (2002).
[105] M. Sadoqi, S. Kumar, and Y. Yamada, J. Thermophys. Heat Transfer **16**, 193 (2002).
[106] M. Prasad, P. F. Conforti, and B. J. Garrison, J. Appl. Phys. **101**, 103113 (2007).
[107] G. Bounos, A. Selimis, S. Georgiou, E. Rebollar, M. Castillejo, and N. Bityurin, J. Appl. Phys. **100**, 114323 (2006).
[108] J. H. Weaver and V. N. Antonov, Surf. Sci. **557**, 1 (2004).
[109] G. Kerner and M. Asscher, Nano Lett. **4**, 1433 (2004).
[110] G. Kerner and M. Asscher, Surf. Sci. **557**, 5 (2004).

Downloaded 11 Oct 2007 to 128.143.68.241. Redistribution subject to AIP license or copyright, see http://jap.aip.org/jap/copyright.jsp